ZNF865 (BLST) Regulates Human Cell Senescence and DNA Damage

Christian Lewis[1], Hunter Levis[1], Jonah Holbrook[1], Jacob T. Polaski[2], Timothy D. Jacobsen[3], Sarah E. Gullbrand[4,5], Brian Diekman[6,7], James C. Iatridis[3], Jason Gertz[1,2,8], Brandon Lawrence[9], Robby D. Bowles[1,9]

[1]University of Utah, Department of Biomedical Engineering, Salt Lake City, UT

[2]Huntsman Cancer Institute, University of Utah, Salt Lake City, UT

[3]Icahn School of Medicine at Mount Sinai, Department of Orthopaedics, New York, NY

[4]University of Pennsylvania, Department of Orthopaedic Surgery, Philadelphia, PA

[5]Corporal Michael J. Crescenz VA Medical Center, Philadelphia, PA

[6]Thurston Arthritis Research Center, University of North Carolina at Chapel Hill, Chapel Hill, NC

[7]Lampe Joint Department of Biomedical Engineering, University of North Carolina at Chapel Hill and North Carolina State University, Raleigh, NC

[8]University of Utah, Department of Oncological Sciences, Salt Lake City, UT

[9]University of Utah, Department of Orthopaedic Surgery, Salt Lake City, UT

One Sentence Summary:

ZNF865 is a modulator of genome stability and senescence and can be used to mediate senescence and DNA damage in aging related diseases such as degenerative disc disease.

Abstract

Senescence has been shown to contribute to the progression of aging related diseases including degenerative disc disease (DDD). However, the mechanisms regulating senescence in the intervertebral disc (IVD) and other tissues/diseases remain poorly understood. Recently, in a CRISPRa genome-wide screen, our lab identified a previously uncharacterized zinc finger protein, ZNF865 (BLST), that regulates a wide array of genes related to protein processing, cell senescence and DNA damage repair. Here, we demonstrate that ZNF865 expression is negatively correlated with age and disease state in human patient IVD samples and mouse IVD. Utilizing CRISPR-guided gene modulation, we show that ZNF865 is necessary for healthy cell function and is a critical protein in regulating senescence and DNA damage in intervertebral disc cells, with implications for a wide range of tissues and organs. We also demonstrate that downregulation of ZNF865 induces senescence and upregulation mitigates senescence and DNA damage in human nucleus pulposus (NP) cells. Importantly, upregulation of ZNF865 shifts the chromatin landscape and gene expression profile of human degenerative NP cells towards a healthy cell phenotype. Collectively, our findings establish ZNF865 as a novel modulator of genome stability and senescence and as a potential therapeutic target for mediating senescence/DNA damage in senescence related diseases and disorders.

Introduction:

Cellular senescence has been increasingly recognized as a key contributor to disease progression in aging related diseases and has been of increasing interest as a therapeutic target. During senescence, cells undergo a state of stable cell cycle arrest often described as a protective mechanism against oncogenic transformation and excessive DNA damage(*1, 2*). These cells often secrete many pro-inflammatory catabolic factors collectively known as the senescence associated secretory phenotype (SASP) that can disrupt the tissue microenvironment and further sustain the inflammatory environment through complex positive feedback loops(*2, 3*). In many aging related disorders, the increased presence of senescent cells is thought to be a major contributor to disease progression. In the central nervous system, the accumulation of senescent glial cells has been shown to contribute to inflammation and neurodegeneration potentially accelerating diseases such as Alzheimer's(*4*) and Parkinson's(*5*). In the lungs, senescent fibroblast populations are associated with impaired repair mechanisms and fibrotic remodeling in pulmonary fibrosis(*6, 7*). In the musculoskeletal system, senescent chondrocytes and other cell types of the joint have been shown to contribute to cartilage matrix breakdown and synovial inflammation in osteoarthritis(*8*) as well as increased inflammation and matrix breakdown in degenerative intervertebral discs (IVD)(*9*). *Copp et al.* showed that chondrocytes obtained from femur cartilage of osteoarthritic patients had significantly higher levels of DNA damage, but also that the amount of DNA damage present in healthy chondrocytes increased with age(*10*), indicating that excessive DNA damage may be an indicator of cells capable of contributing to disease pathology in osteoarthritis, and other musculoskeletal disorders.

Back pain is one of the most common musculoskeletal disorders and a leading cause of disability worldwide(*11*), with a large population of people expected to experience it at some point

in their lifetime(*12, 13*). Back pain incidence and severity have been shown to increase with age with 40% of back pain attributed to degenerative disc disease (DDD)(*14*). While back pain etiology is diverse and multifactorial, growing evidence suggests biological aging and senescence is one of the major contributing factors. Traditionally DDD onset is associated with the breakdown of the disc tissue due to genetics(*15*), aging(*16*), loading history(*17*) and inadequate metabolite transport(*18*). However, as DDD progresses, studies have shown there is decreased cell activity due to increased cell senescence(*19, 20*). Additionally, degenerative discs are often characterized by increased presence of pro-inflammatory cytokines, proteases and pain related growth factors consistent with the SASP phenotype. These changes to extracellular matrix composition can lead to mechanical instability, pain and disability rates(*18, 21-23*).

Targeting senescent cells via senolytics within the IVD has provided promising results in reducing the release of SASP factors in isolated IVD cells and intact human IVDs(*24, 25*). Oral administration of the senolytics o-vanillin and RG-7112 resulted in decreased pain and histological degeneration in the IVD of sparc null mice(*26*). Additionally, intra-peritoneal delivery of the senolytics dasatinib and quercetin from 14 to 23 months of age significantly improved nucleus pulposus and annulus fibrosis outcomes in wild type mice(*27*). Overall, this work further distinguishes cellular senescence as an important mediator of IVD degeneration and highlights the critical need to develop novel tools that target senescence directly to prevent degeneration and reduce pain caused by SASP.

Recently, in a genome wide CRISPRa perturbation screen we identified the ZNF865 gene, also known as BLST(*28*), that we used as a cell engineering tool to enhance tissue deposition and mechanical properties of engineered intervertebral discs(*28*). ZNF865 regulates a wide array of genes associated with senescence and DNA damage but has not been functionally characterized.

ZNF865 is a C2H2 ZNF that is 1059 amino acids long, containing six disordered regions, twenty unique ZNF domains, two transactivation domains (TADs) and two TGEKP linkers (**Figure 1A**). The presence of the two TADs indicate that ZNF865 likely stimulates transcriptional activity by interacting with transcriptional regulators(*29*). Despite broad expression across all cell types (**Figure 1B**), there are no publications with functional characterization of the biological role of ZNF865. Additionally, a rare disease mutation in ZNF865 is associated with a wide range of symptoms including global developmental delay, joint hypermobility, muscle hypertonia, loose inelastic skin, hand tremors, and eye/ear/brain abnormalities indicating effects across a wide range of tissues and organs in human patients(*30*). To this end, additional investigation of ZNF865 will provide fundamental knowledge of the cellular and molecular pathways regulated by ZNF865.

Here we investigated ZNF865 function in the context of DDD and identified the primary function of this gene in the regulation of senescence and DNA damage. This investigation of DNA damage further elucidated the role DNA damage plays in the onset and perpetuation of the degenerative phenotype in DDD, which had previously not been studied. Furthermore, these insights identify ZNF865 as a key modulator in maintaining genomic stability and as a potential therapeutic target in other aging related diseases hallmarked by senescence.

Results

ZNF865 upregulation alters related cell functions across multiple cell types

To begin investigating the molecular role of ZNF865, CRISPR activation (CRISPRa) was used to increase the expression of ZNF865 using the dCas9-VPR system alongside a non-target control (**Figure 1C,1D**). RNAseq was then performed on three different human cell types; human embryonic kidney cells (HEK293), adipose derived stem cells (ASCs) and degenerative human nucleus pulposus cells (dhNPCs), and comparisons were made across the CRISPRa ZNF865 and non-target samples (**Figure 1E, 1F, 1G**). Upregulation of ZNF865 in each of these cell types showed 2,699, 6,647 and 1,752 significantly differentially expressed genes, respectively. Utilizing Enrichr(*31*), further analysis of these genes showed a number of significantly differentially regulated molecular processes using the KEGG 2021 Human Pathway that were shared across cell types (**Figure 1H, 1I, 1J, Table S1-S3**)(*32*). The notable pathways across all three cell types included cell cycle, DNA replication, cellular senescence, mismatch repair, p53 signaling, mTOR signaling, base excision repair, and homologous recombination. The shared molecular processes suggested a role for ZNF865 in regulating cell division, DNA repair, and senescence.

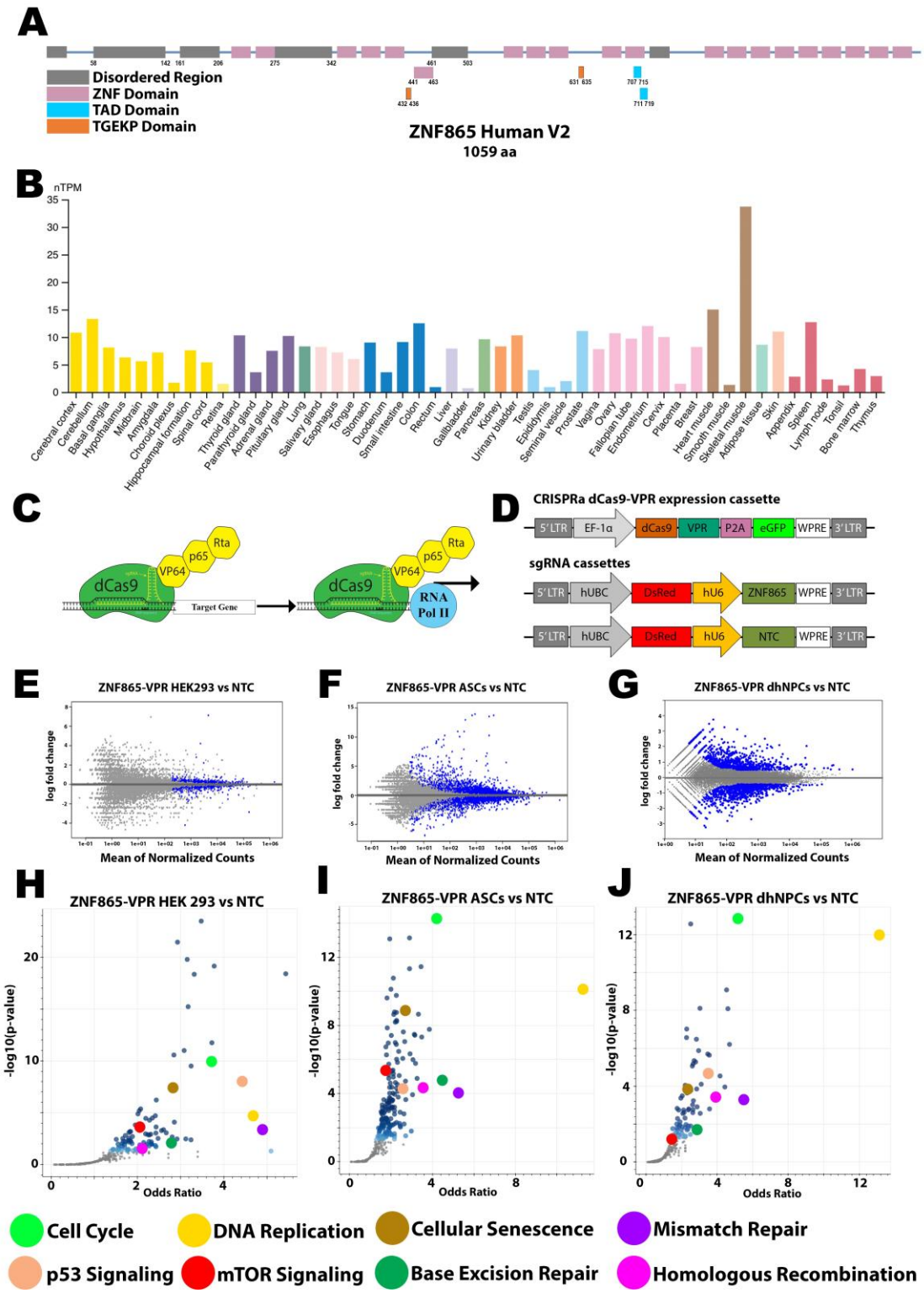

Figure 1: ZNF865 Regulates Similar Gene Networks Across Multiple Cell Types. A Structure of the human ZNF865 gene. **B** ZNF865 expression across different human tissue sources. nTPM = normalized transcripts per million. **C** dCas9-VPR CRISPRa system and **D** plasmid maps for lentiviral delivery targeting ZNF865 or NTC. **E** MA plots from RNA-seq on ZNF865 upregulated HEK293 cells, **F** ASCs and **G** human dhNPCs. **H** Volcano plots showing the top common molecular process affected by ZNF865 upregulation across HEK293 cells, **I** ASCs and **J** human dhNPCs using the KEGG 2021 Human Pathway. *NTC is non-target control.*

ZNF865 expression is correlated with human degenerative disc disease and aging

To evaluate whether ZNF865 expression is pathologically relevant within degenerative disc disease, gene expression was measured via qRT-PCR on dhNPCs from patients undergoing surgical treatment for low back pain, and healthy NP cells (hNPCs) from trauma patients at first passage after plating in vitro (**Figure 2A**). We observed a strong correlation (R^2=0.94, p=0.0281) between ZNF865 expression and age in hNPCs and significantly decreased expression in dhNPC samples at matched ages (**Figure 2B**). Immunofluorescence staining for ZNF865 matched the qRT-PCR data with significantly less ZNF865 staining in dhNPC samples compared to hNPCs (**Figure 2C,2D**). ZNF865 staining was localized to the nucleus of the cells, consistent with bioinformatic predictions that ZNF865 is a transcription factor. Of note, 28.7% of hNPCs stained for ZNF865, while only 16.8% of dhNPCs were stained, indicating that ZNF865 may not be expressed by all cells at a detectable level at a given time (**Figure 2E**).

To determine whether expression of this gene also changes in mouse IVD, ZFP865 expression (mouse orthologue of ZNF865)(*33*) was in the caudal NP of mice at 4, 12 and 24 months of age (**Figure 2F**). These results were consistent with the human data, where ZFP865 expression decreased with increasing age. Both population average expression level (**Figure 2G**) and percentage of cells expressing (**Figure 2H**) showed decreases, with a strong negative correlation between cells expressing ZFP865 and age in the mouse (r = -0.9976, p = 0.04435).

Cell senescence has been proposed as a potential mechanism of disc degeneration with degenerative discs showing increased levels of senescence (**Figure 2I)**(*19, 20*). However, the functional and molecular links between senescence and DDD are still relatively unknown. Given that our RNA-seq data indicates that both senescence and closely associated DNA repair pathways are significantly altered following CRISPRa ZNF865 upregulation (**Figure 1J**), we investigated

DNA damage in the human dhNPCs and hNPCs using alkaline comet assays. Here we observed that the percentage of DNA damage in the comet tail in dhNPCs was significantly higher than in hNPCs (**Figure 2J, 2K**). Taken together, this data indicates a relationship between ZNF865 expression and DDD, as well as DDD progression and DNA damage. Moving forward we investigated the relationship between ZNF865 expression and cellular senescence and DNA damage in human NP cells.

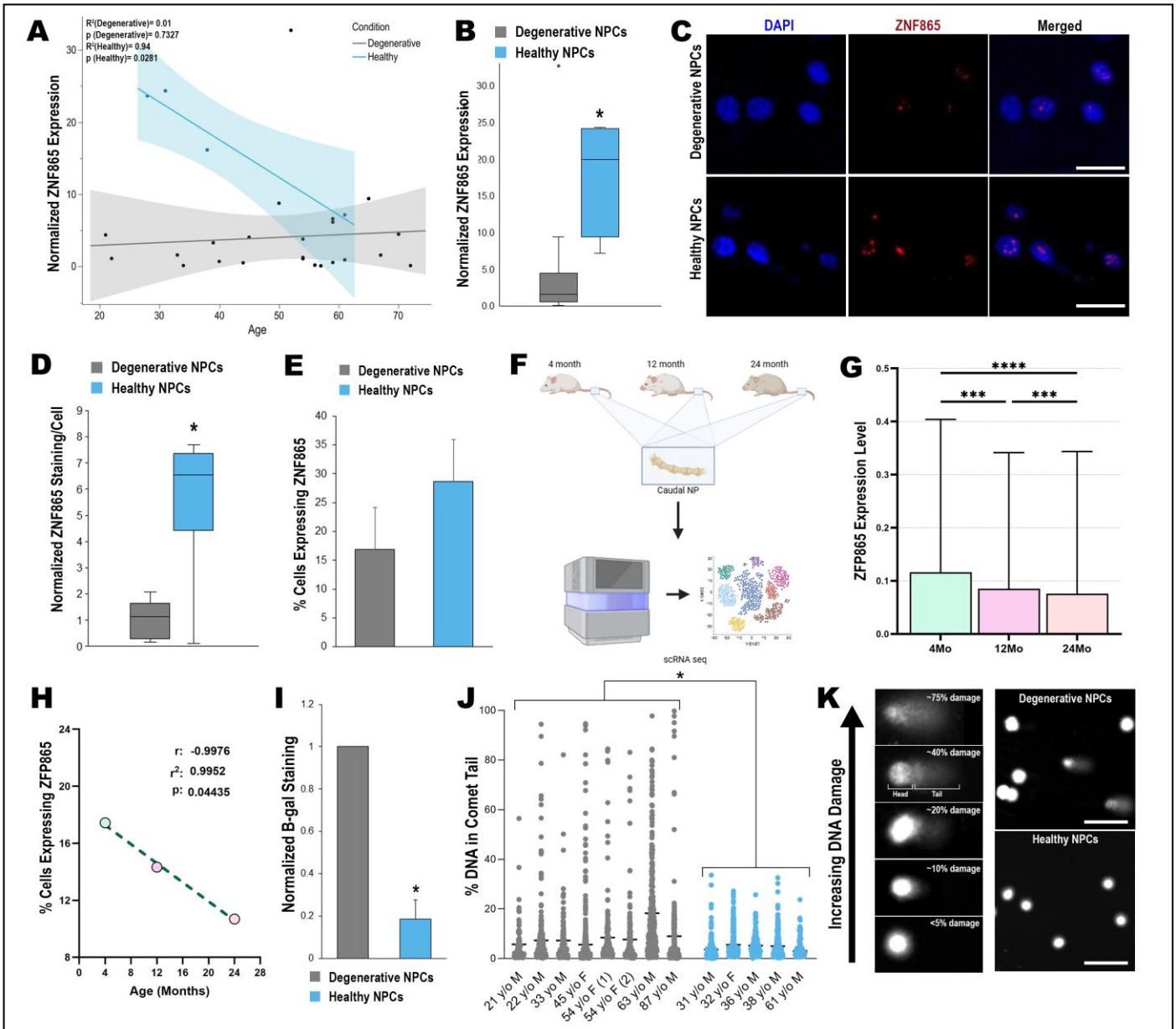

Figure 2: ZNF865 Expression is Correlated with Aging, Degeneration, and DNA Damage in Human and Mouse NP cells. A Normalized ZNF865 expression in hNPCs (n=4) and dhNPCs (n=23) in individual patients and **B** grouped by pathology. **C** Representative images from ZNF865 immunofluorescence staining (Blue=DAPI, Red=ZNF865). **D** ZNF865 immunofluorescence staining per cell normalized to the dhNPC level (n=7). **E** Percent of dhNPCs and hNPCs expressing ZNF865 from immunofluorescence staining (n=3-4). **F** Workflow for scRNA-seq in the caudal NP of aging mice. **G** ZFP865 expression level in the caudal NP of aging mice. **H** Percent of cells positive for ZFP865 in the aging mouse model. **I** Normalized β-galactosidase staining of healthy (n=4) and dhNPCs (n=5). **J** Percent DNA in the comet tail of naïve hNPCs (n=5) and dhNPCs (n=8) measured by comet assay. **K** Images showing single cell comets with percent damage, and representative dhNPCs and hNPC examples. (*Scale bars = 50 μm. significance *=p<0.05, **=p<0.01, ***=p<0.001*)

CRISPRa/i allows for highly titratable expression of ZNF865

CRISPRa systems, such as dCas9-VPR, have been shown to increase the expression of targeted genes by recruiting transcriptional coactivators(*34*) (**Figure 3A**). Alternatively, CRISPR interference systems, such as dCas9-KRAB, have previously been shown to suppress gene expression by trimethylation of the histone at the targeted location to prevent transcription at a desired location(*35*) (**Figure 3B**). Specifically, when targeting ZNF865 we have shown that depending on the gRNA used, expression is titratable in both positive and negative directions (**Figure 3C**). Upon downregulation of ZNF865 in hNPCs with the gRNA that showed the highest level of repression, there was a significant decrease in the amount of ZNF865 protein as measured by immunofluorescence staining (**Figure 3D,3E**). Upon upregulation of ZNF865 in dhNPCs with the gRNA that showed the highest level of activation, there was a significant increase in the amount of ZNF865 protein (**Figure 3D, 3F**).

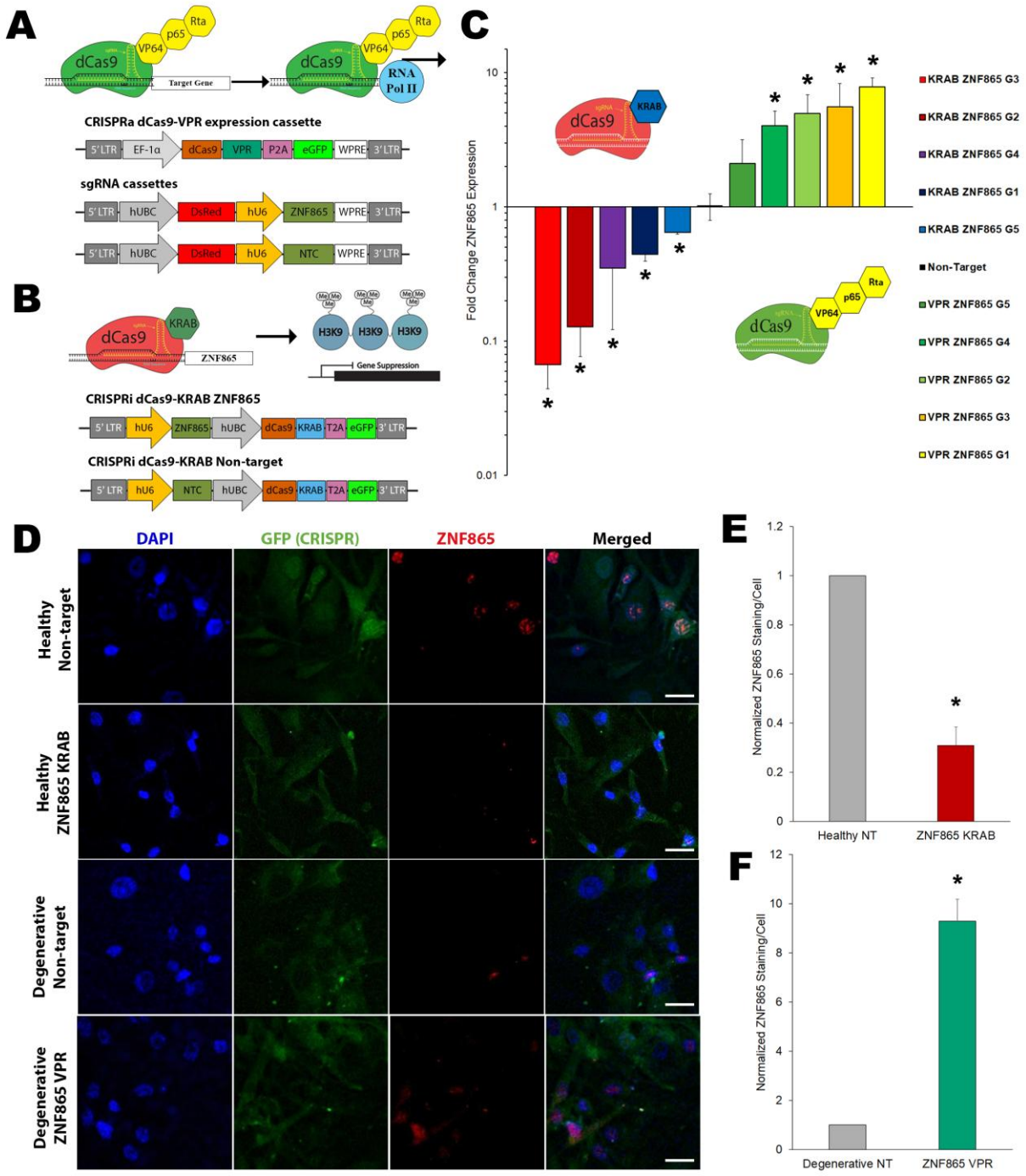

Figure 3: ZNF865 is titratable in Human NP cells with CRISPRi and CRISPRa. A dCas9-KRAB repression system with plasmid maps used for CRISPRi of ZNF865 or non-target. **B** dCas9-VPR activation system and plasmid maps used for CRISPRa of ZNF865 or non-target. **C** Fold change ZNF865 expression when using CRISPRi or CRISPRa systems in ASCs (n=4-5). **D** Representative immunofluorescence images after transduction with CRISPRi/CRISPRa systems with ZNF865 or non-target. **E** Normalized ZNF865 immunofluorescence staining per cell when using the CRISPRi (n=3-4) and **F** CRISPRa systems with the top performing gRNAs (n=4-5) (*Scale bars = 50 µm. significance *=p<0.05)*

ZNF865 downregulation in healthy human NP cells induces senescence and DNA damage

hNPCs were isolated from discarded surgical tissue from deidentified trauma patients and transduced with the CRISPRi vector targeting ZNF865 (ZNF865 KRAB) or a non-target control (**Figure 4A**). Following successful transduction cells were monitored for cell proliferation over 6 days. Samples transduced with ZNF865 KRAB showed decreased proliferative capacity compared to cells transduced with the non-target vector (**Figure 4B**). To determine if the reduction in cell growth observed in the ZNF865 KRAB samples was consistent with entry into senescence, hNPCs were stained for key markers of cellular senescence, including senescence associated β-galactosidase (β-gal), $p16^{INK4A}$ (p16) and $p21^{waf1/Cip1}$ (p21). The ZNF865 KRAB NP cells showed significantly higher levels of all three senescence markers, with 5.4-fold, 4.7-fold, and 6.9-fold increases in staining, respectively (**Figure 4C-4E, 4H**). Entry into senescence has commonly been linked to increased DNA damage as a way to prevent damaged cells from perpetuating their genomes in division(*2, 36*), and ZNF865 regulation had been demonstrated to regulate DNA damage repair pathways (**Figure 1**). To quantify the amount of DNA damage across patient samples, we performed alkaline comet assays 3 weeks after transduction. Here, the ZNF865 KRAB NP cells showed significantly higher levels of DNA damage compared to the non-target samples, indicating a functional connection between decreased ZNF865 expression and DNA damage (**Figure 4F,4G**). This data is consistent with the relationships observed between ZNF865 and senescence and DNA damage in human patient nucleus pulposus cells (**Figure 2**) and our RNAseq data (**Figure 1**).

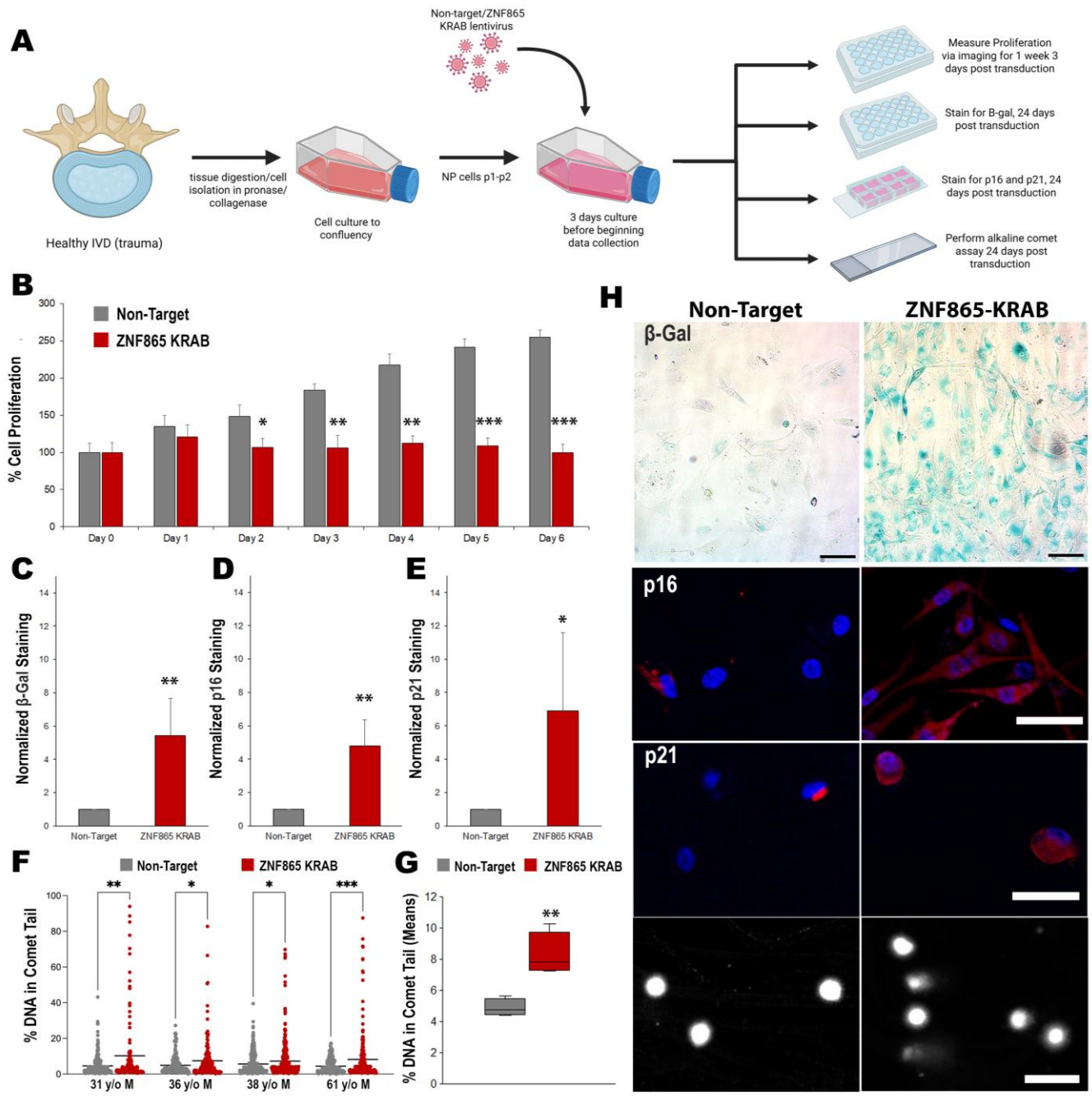

Figure 4: CRISPRi of ZNF865 decreases proliferation rates, increases senescence and increases DNA damage in hNPCs. A Workflow for CRISPRi of ZNF865 or non-target in hNPCs. **B** Quantified cell proliferation of healthy human non-target and ZNF865-KRAB NP cells (n=4). **C** SA-β-Galactosidase, **D** p16 and **E** p21 staining normalized to non-target (n=4). **F** Percent DNA in comet tail in individual patients obtained by comet assay. **G** Donor mean percent DNA in comet tail (n=4). **H** Representative images from SA-β-Galactosidase, p16 and p21 staining, and nuclei from comet assays. (Scale bar β-Gal = 100 *µm, scale bar others = 50 µm. Significance *=p<0.05, **=p<0.01, ***=p<0.001*)

ZNF865 upregulation in degenerative human NP cells decreases senescence, SASP phenotype and DNA damage

To begin studying the effects of ZNF865 regulation in pathologic cells, dhNPCs were isolated from discarded surgical tissue from deidentified patients undergoing surgical treatment for chronic back pain. Cells were then transduced with ZNF865 upregulation cassettes (ZNF865-VPR) or a non-target control (**Figure 5A**). Following successful transduction, cells were monitored for cell proliferation via fluorescent imaging over the course of 5 days. We observed significant increases in cell growth within 3 days in the ZNF865-VPR cells compared to the non-target controls (**Figure 5B**). This led to a significant decrease in doubling time in the ZNF865-VPR dhNPCs compared to the non-target dhNPC controls, at 2.49 days and 4.09 days respectively, with non-significant differences compared in the naïve hNPCs with a doubling time of 3.2 days (**Figure 5C**). We stained each treatment group for key senescence markers 10 days after transduction. Here the non-target dhNPCs showed the highest levels of staining in β-gal, p16 and p21, with significantly lower levels of senescence staining in the ZNF865-VPR dhNPCs and hNPCs. Additionally, the ZNF865-VPR dhNPCs and hNPCs were non-significantly different from each other (**Figure 5D-5G**).

To assess the ability to directly regulate DNA damage, we performed alkaline comet assays. Here we found that upregulation of ZNF865 significantly decreased the percentage of DNA in the comet tails in all patients, with five of the seven patients reaching significance (**Figure 5I**). When the mean damage of each donor is considered, there is a significant decrease in the ZNF865-VPR dhNPCs compared to the non-target controls, with the ZNF865-VPR dhNPCs matching the healthy controls (**Figure 5H,5I**). This demonstrates ZNF865's ability to directly regulate DNA damage and senescence observed in human samples from painful degenerative discs.

To better understand the downstream effects of reversing senescence and DNA damage in these cell populations, a Luminex assay was run on 10 SASP related proteins using the cell culture supernatant from the ZNF865-VPR dhNPCs, non-target control dhNPCs, and naïve hNPCs. Nine of the ten analytes including IL-1β, IL-6, TNF-α, IL-8, MMP-1, MMP3, MMP-12, NGF-β and VEGF-a in the ZNF865-VPR showed significant decreases in concentration compared to the non-target control, with the non-significant difference in MCP-1 trending towards a reduced level (**Figure 5J**). From the Luminex assay, a composite normalized SASP score was created that weighs each analyte equally and is normalized to the hNPC supernatants. Here, we saw significant differences in SASP score between the ZNF865-VPR dhNPCs and non-target control dhNPCs, as well as significant differences between the non-target control dhNPCs and hNPCs. The ZNF865-VPR dhNPCs had a SASP score that was slightly higher than the hNPCs, but this difference was not statistically significant (**Figure 5K**). This indicates that increased expression of ZNF865 leads to a decreased SASP profile and a secretome more similar to hNPCs.

To assess ZNF865 regulation on ECM deposition within the disc, 3D pellet culture was performed using non-target dhNPCs pooled from three patient samples, and two ZNF865-VPR dhNPC patient samples (**Figure 5L**). After 3 weeks of culture, we saw significant increases in collagen production in both ZNF865-VPR patients compared to the pooled non-target pellets, with no significant increases in glycosaminoglycan (GAG) production (**Figure 5M,5N**). From these measurements, a composite anabolic score was created, weighing both collagen production and GAG production equally and normalizing to the non-target samples. Here we saw significant differences in anabolic score for both ZNF865-VPR samples compared to the non-target (**Figure 5O**). Additionally, when plotting the SASP scores and anabolic scores from both patients on the same plot we see a clear separation between the non-target samples and the ZNF865-VPR samples

(**Figure 5P**), indicating that ZNF865 upregulation results in decreased inflammation as well as increased ECM deposition capabilities.

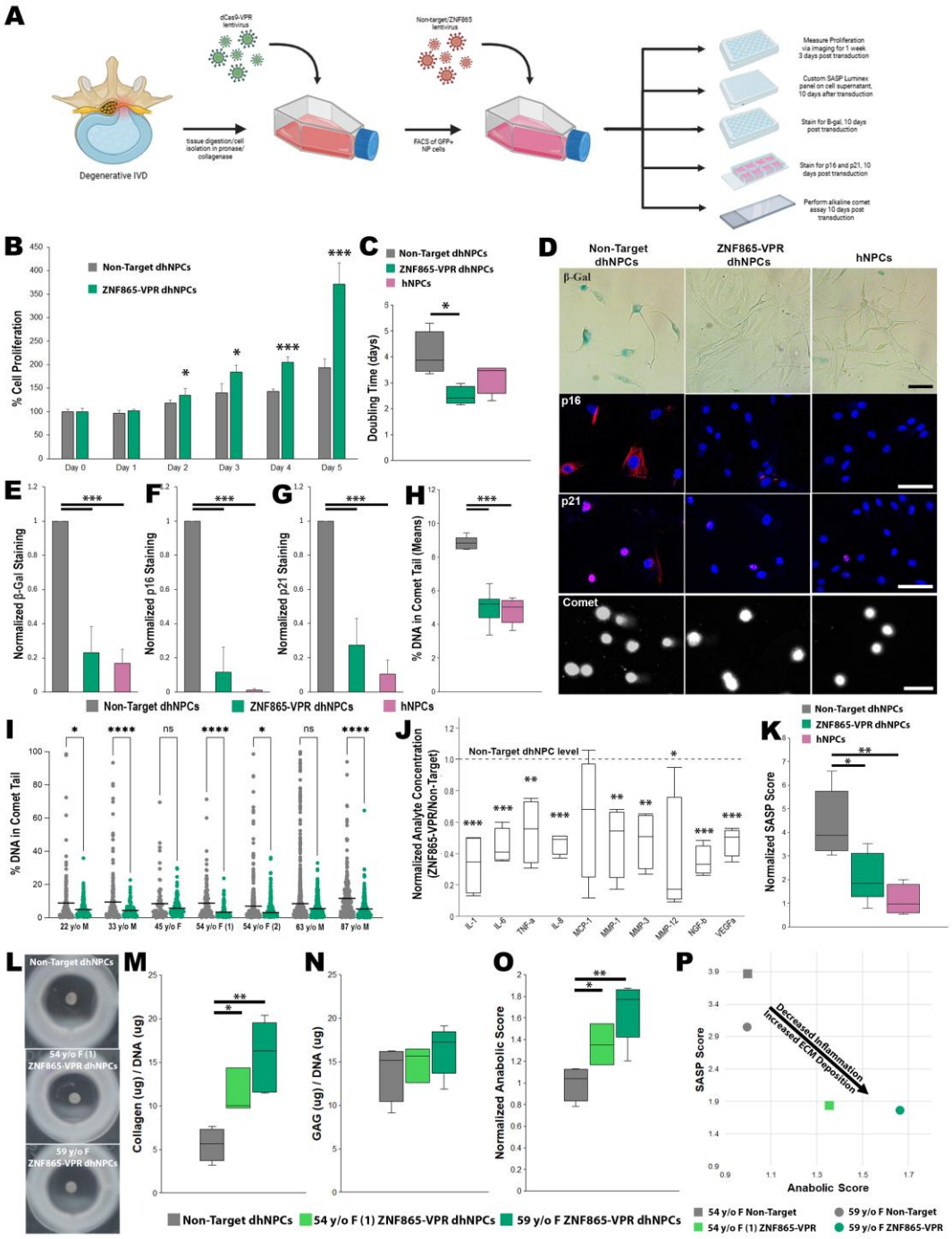

Figure 5: CRISPRa of ZNF865 restores proliferation, decreases senescence, decreases SASP phenotype and decreases DNA damage to healthy levels in dhNPCs. A Workflow for CRISPRa of ZNF865 or non-target in dhNPCs. **B** Quantified cell proliferation of human non-target dhNPCs and ZNF865-VPR dhNPCs (n=5). **C** Doubling times of non-target dhNPCs, ZNF865-VPR dhNPCs and hNPCs (n=5). **D** Representative images from β-Gal, p16 and p21 staining, and nuclei from comet assays. **E** SA-β-Galactosidase, **F** p16 and **G** p21 staining normalized to non-target (n=4-5). **H** Percent DNA in comet tail in non-target dhNPCs, ZNF865-VPR dhNPCs and hNPCs. **I** Donor mean percent DNA in comet tail (n=7). **J** Analyte concentration for SASP related inflammatory cytokines, proteases and proteins present in ZNF865-VPR dhNPCs normalized to non-target samples (n=4). Non-target levels indicated by dashed line. **K** SASP score normalized to hNPC values (n=4-5). **L** Representative images of pellet culture. **M** Total collagen production per DNA and **N** GAG production per DNA and **O** normalized anabolic scoring from pellet culture in pooled non-target dhNPCs and two ZNF865-VPR dhNPC patient samples (n=3-6). **P** Plot of showing relationship of SASP score and anabolic score after ZNF865 upregulation. Scale bars = *50 µm. Significance *=p<0.05, **=p<0.01, ***=p<0.001*)

ZNF865 upregulation in degenerative NP cells restores healthy chromatin state

We next sought to identify changes in gene expression and chromatin accessibility with potential functional importance for DDD-associated phenotypes. To this end, we performed both RNA-seq and ATAC-seq using healthy (hNPCs) and degenerative (dhNPCs) patient samples as well as degenerative samples with CRISPR-activated ZNF865 (ZNF865 VPR dhNPCs) **(Table S4,S5)**. Principal component analysis using these cohorts **(Figures 6A-6B)** shows that ZNF865 expression causes dhNPCs to become more related to hNPCs, suggesting CRISPRa of ZNF865 restores some molecular features of hNPCs. RNA-seq identified many changes in gene expression that differentiate hNPCs from dhNPCs (7924 genes) and ZNF865 VPR dhNPCs from dhNPCs (1984 genes). ATAC-seq also revealed changes in genome-wide chromatin accessibility when comparing hNPCs to dhNPCs (979 total sites) and ZNF865 VPR dhNPCs to dhNPCs (593 total sites). To associate specific genes with the observed changes in chromatin accessibility, we used Genomic Regions Enrichment of Annotations Tool (GREAT)(*37*). In total, we found 1463 unique genes associated with changes in chromatin accessibility when comparing hNPCs to dhNPCs and 949 unique genes when comparing ZNF865 VPR dhNPCs to dhNPCs.

To assess concordance between differentially expressed genes identified by RNA-seq and genes associated with changes in chromatin accessibility by ATAC-seq, we employed hypergeometric tests to quantify the degree of overlap between either upregulated or downregulated genes and genes associated with either increased or decreased chromatin accessibility. This analysis revealed statistically significant enrichment in the number of shared genes compared to what would be expected by chance across all comparisons **(Figure 6C)**. Specifically, we found 184 upregulated/increased accessibility and 84 downregulated/decreased accessibility genes that are shared between comparisons of hNPCs and dhNPCs, representing >3-

fold and >2-fold enrichment compared to the amount of overlap expected by chance, respectively. Similarly, we found 51 upregulated/increased accessibility and 33 downregulated/decreased accessibility genes that are shared between comparisons of ZNF865 VPR dhNPCs and dhNPCs, representing >6-fold and >5-fold enrichment over the amount of overlap expected by chance, respectively.

Within the individual genes, there are several notable examples, including *COL6A2* **(Figure 6D)**, which was recently implicated as a potential marker of DDD(*38*). Normalized counts from RNA-seq show upregulation of *COL6A2* in both hNPCs and ZNF865 VPR dhNPCs, compared to dhNPCs. These differences in *COL6A2* expression correlate with changes in chromatin accessibility, where we observed more prominent ATAC-seq peaks in both hNPCs and ZNF865 VPR dhNPCs compared to dhNPCs **(Figure 6E)**. We also found that *USP12*, which has a known functional role as an inflammatory mediator involved in MMP production(*39*), is downregulated in both hNPCs and ZNF865 VPR dhNPCs compared to dhNPCs **(Figure 6F)**. These differences in expression correlate with changes in chromatin accessibility, where both hNPCs and ZNF865 VPR dhNPCs show less prominent ATAC-seq peaks compared to dhNPCs **(Figure 6G)**. Collectively, these results provide evidence that ZNF865 shifts dhNPCs toward a healthier molecular phenotype.

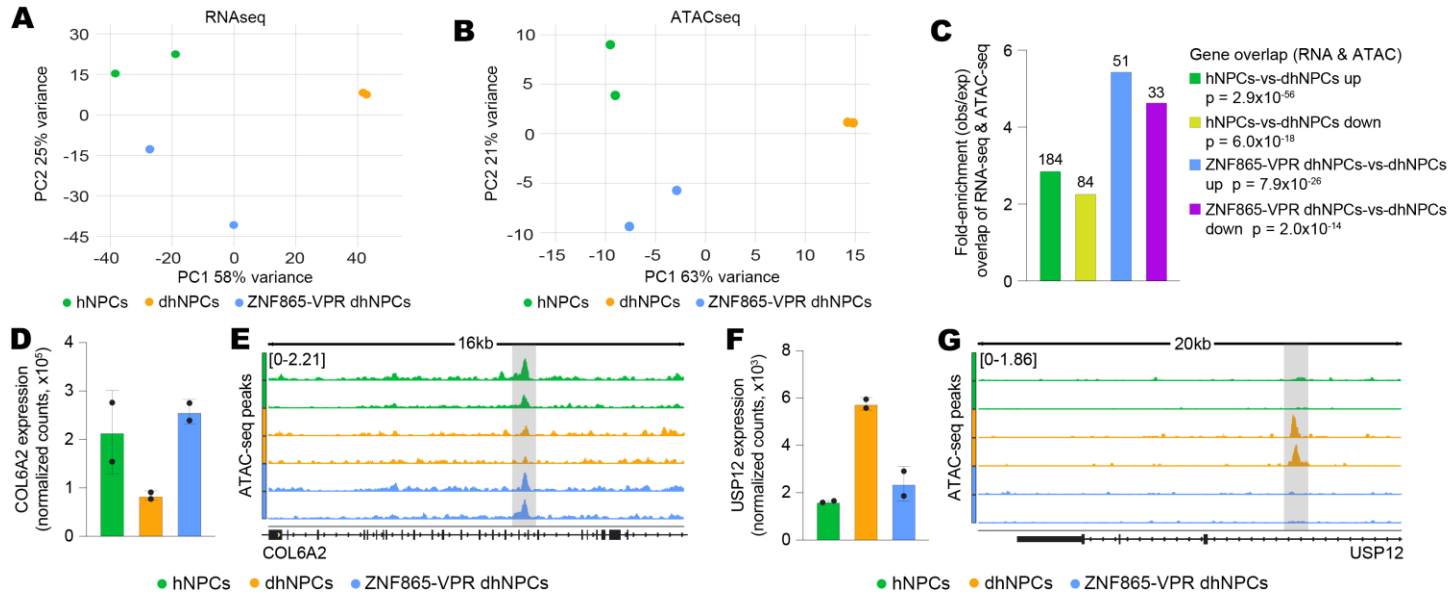

Figure 6: CRISPRa of ZNF865 returns human NP cells to healthy chromatin state and gene expression. A Principal component analysis of RNA-seq data shows the relationship between hNPCs (green circles), dhNPCs (orange circles), and ZNF865 VPR dhNPCs (blue circles). **B** Principal component analysis of ATAC-seq data shows the relationship between hNPCs (green circles), dhNPCs (orange circles), and ZNF865 VPR dhNPCs (blue circles). **C** Hypergeometric test results are shown as a bar plot to quantify the degree of gene-level overlap of RNA-seq and ATAC-seq datasets between comparisons of hNPCs and dhNPCs (green and yellow bars) and ZNF865 VPR dhNPCs and dhNPCs (blue and purple bars). Bars corresponding to the number of shared upregulated genes from RNA-seq and genes associated with increased chromatin accessibility from ATAC-seq for each comparison are denoted as "up." Conversely, bars corresponding to the number of shared downregulated genes from RNA-seq and genes associated with decreased chromatin accessibility from ATAC-seq for each comparison are denoted as "down." **D** Browser tracks display differences in ATAC-seq peaks (shaded region) in *COL6A2* from hNPCs, dhNPCs, and ZNF865 VPR dhNPCs. The colors of the tracks correspond to the bars in panel D. **E** Bar plot illustrates the differences in USP12 expression between hNPCs (green), dhNPCs (orange), and ZNF865 VPR dhNPCs (blue) using normalized counts from RNA-seq. **F** Browser tracks display differences in ATAC-seq peaks (shaded region) in USP12 from hNPCs, dhNPCs, and ZNF865 VPR dhNPCs. The colors of the tracks correspond to the bars in panel F.

Discussion

Despite the broad expression of ZNF865 across all cell types(*40*), this study represents the first functional characterization of the ZNF865 gene. Through CRISPRa-mediated upregulation in three distinct cell types; *HEK293* cells, *ASC*s, and human NP cells, we identified a set of consistently enriched processes involving cellular senescence, DNA repair mechanisms, and cell cycle regulation pathways. These shared processes suggest that ZNF865 may act as a core regulator of molecular processes that underlie cell senescence and genomic stability.

We demonstrated that ZNF865 expression is reduced in human DDD samples, and that this reduction is associated with increased levels of DNA damage and cell senescence. Here we show that patient derived dhNPCs had significantly lower ZNF865 gene expression, lower protein levels, and greater DNA damage compared to hNPC controls, highlighting a potential connection between ZNF865 depletion and disc degeneration. This data is supported by the single cell RNA sequencing of the caudal NP of aging mice *in vivo,* which showed a parallel decline in ZFP865 expression and the proportion of cells expressing ZFP865 with increased age. Together, this data suggests that the loss of ZNF865 or orthologues may represent a feature of disc tissue aging, potentially contributing to aging related phenotypes such as cell senescence and the lack of regenerative capacity of the disc.

CRISPR-based gene modulation systems such as CRISPRa and CRISPRi offer a method for modulating the expression of ZNF865, allowing us to define its functional roles. Using these CRISPR based gene modulation systems revealed that expression of ZNF865 is highly tunable and can lead to robust functional differences(*28*), with gene expression shown to be associated with proliferation and cell cycle progression. Downregulation of ZNF865 in hNPCs led to reduced proliferation, increased senescence, and elevated DNA damage, all of which are features

commonly associated with tissue degeneration and DDD. Conversely, when ZNF865 was upregulated in dhNPCs, these phenotypes were reversed, with increased proliferation rates, decreased senescence marker staining, and decreased DNA damage. This also led to a significant reduction in many SASP factors such as proinflammatory cytokines (IL-1, IL-6, TNF-α, IL-8), proteases (MMP-1, MMP3, MMP12), and pain related growth factors (NGF, VEGF) commonly associated with DDD. After upregulation of ZNF865, these dhNPCs showed cell phenotypes more similar to the hNPCs. Additionally, in 3D pellet culture ZNF865 upregulation showed increased ECM deposition capability and allowed for a greater number of pellets to be created with a single patient compared to the non-target dhNPCs which required 3 patient cells to be pooled.

These phenotypic differences between patient samples are consistent with gene regulatory changes. Both RNA-seq and ATAC-seq showed that CRISPRa of ZNF865 recapitulated some global features of gene expression and chromatin accessibility found in hNPCs. This effect can be seen at the level of individual genes, where we observed many up- and down-regulated genes that also harbored sites of more open and closed chromatin. One notable example we identified is *COL6A2,* whose expression is higher in hNPCs and ZNF865 VPR dhNPCs compared to dhNPCs. This gene encodes a type VI collagen chain, revealing a potential genetic link with increased ECM deposition by ZNF865 VPR dhNPCs in 3D pellet culture. Overall, these data highlight concordant changes in phenotypes and gene regulation, where our data suggests ZNF865 drives an overall shift of both gene expression and chromatin state toward that of healthy NP cells.

Collectively, this data suggests that ZNF865 plays a fundamental role in DDD and aging, specifically in maintaining genetic stability through DNA repair mechanisms that prevent the onset of senescence. The rescue of dhNPCs from a senescent phenotype upon ZNF865 upregulation not only points to the importance of ZNF865 within the degenerative phenotype but also identifies

ZNF865 as a potential therapeutic target for DDD. Previously, we demonstrated upregulation of ZNF865 in multiplex with ACAN and Col2a1 was shown to enhance functional tissue deposition and improve biomechanical properties of human-scale engineered discs(*28*). This suggests that in addition to decreasing inflammatory pathways caused by DNA damage and SASP, CRISPR gene therapies using ZNF865 have potential to be used in multiplex for a wide variety of purposes including increased protein production or mechanical properties of engineered tissues. However, additional studies need to be conducted to better understand how and why these changes occur.

This work also offers broader implications for other aging related degenerative diseases, where controlling cellular senescence and SASP may be paramount to understanding and slowing disease progression. Ultimately, preventing senescence may improve the health span of individuals by preventing the onset of many musculoskeletal disorders, or neurodegenerative disorders. ZNF865 was recently identified independently in a family of zinc finger proteins where increased gene expression was associated with better prognosis in esophageal cancer(*41*), indicating that it may be a useful clinical target for understanding cancer progression. ZNF865 was also identified as a potentially relevant target in Parkinson's disease(*42*). *Liu et al.* suggested that ZNF865 protein can alleviate damage caused by Parkinson's disease by preventing apoptosis and enhancing motor neuron performance(*42*). Within our RNA sequencing data, a number of neurodegenerative diseases such as ALS, Parkinson's and Alzheimer's were listed as top pathways effected by upregulation of ZNF865, suggesting that targeting ZNF865 or its downstream pathways could represent a strategy for restoring tissue function in aging related degenerative diseases. Additionally, outside of human pathology, ZNF865 regulation has potential to be used in a wide range of manufacturing spaces by increasing cell proliferation or protein production. The work presented here and in *Levis et al.* shows that upon upregulation of ZNF865, significant increases

in cell proliferation can be achieved in a range of different cell types and result in increased protein production(*28*).

This work indicates ZNF865 as an important gene for healthy cell function and genome maintenance. However, key questions remain that need to be clarified in future experiments. Identification of the upstream regulators and downstream effectors will allow for better regulatory networks to be established around ZNF865 and help to define what molecular interactions are leading to observed results. This will also allow for the development of blocking antibodies, inhibitors or activators that could allow for enhanced control of ZNF865 regulation outside of using CRISPR based therapies. This work uses DDD as a model system for understanding DNA damage and senescence regulation by ZNF865, however, additional primary cell types and disease models should be considered to establish a broader understanding of the functional role that ZNF865 plays within aging related diseases.

Overall, this work also highlights the use of CRISPR gene modulation strategies for probing unknown gene function and identifies ZNF865 as an important gene in regulating cell cycle and DNA repair mechanisms, with significant implications for DDD and other senescence associated degenerative disorders. This study serves as a first step in understanding the basic biology of the ZNF865 gene and establishes the importance of understanding ZNF865 dysregulation for both disease pathology, and as a potential therapeutic target for senescence associated disorders.

Materials and Methods

Experimental overview

CRISPRa was used to upregulate the expression of ZNF865 in HEK 293 cells, ASCs and human dhNPCs and investigated for changes in gene expression via RNAseq. Next, ZNF865 expression and DNA damage were examined in healthy and dhNPCs to investigate DDD pathology. An aging mouse model from *Jacobsen et al.* was used to investigate an identified orthologue for ZNF865 expression changes with aging(*43*). CRISPRi was then used to downregulate the expression of ZNF865 in hNPCs to investigate differences in proliferation, senescence and DNA damage as a result of decreased expression. Finally, CRISPRa was used to upregulate the expression of ZNF865 in dhNPCs to investigate differences in proliferation, senescence, SASP expression, DNA damage and chromatin accessibility as a result of increased expression.

General cell culture

All cell culture was performed in standard culture conditions (21% O_2, 5% CO_2, 37°C), with media changes every 2-3 days. *HEK 293*: Complete growth medium for cell culture for HEK 293 (ATCC CRL-1573) cells consists of HG-DMEM (ThermoFisher Scientific, Waltham, MA) supplemented with 10% fetal bovine serum (FBS) (ThermoFisher Scientific), 25µg/mL gentamicin (Corning), and 25mM HEPES (ThermoFisher). *hASC:* Complete growth medium for culturing of human adipose derived stem cells (ASCs, ATCC SCRC-4000) consists of Lonza ADSC Basal Medium (Lonza, Lexington, MA PT-3273), 10% MSC FBS (ThermoFisher Scientific), 5mL GlutaMax (ThermoFisher Scientific), 30µg/mL Gentamicin (Corning), and 15ng/mL Amphotericin (ThermoFisher Scientific). *hNPCs:* Primary human nucleus pulposus cells (hNPCs)

were cultured in complete growth medium containing DMEM-HG (ThermoFisher Scientific) supplemented with 10% FBS (ThermoFisher Scientific), 50µg/mL gentamicin (Corning), 25mM HEPES (ThermoFisher Scientific), and 2ng/mL of recombinant human fibroblast growth factor-basic (rhFGF, Peprotech, Cranbury, NJ, 100-18C).

gRNA design

Upregulation gRNA design was performed using Genome Target Scan 2 and ChopChop(*44, 45*). The 5'-UTR, the promoter region up to 500bp upstream of the ZNF865 transcription start site (TSS), and up to 500bp upstream of the second exon were analyzed for gRNAs. The top 6 gRNAs from each analysis tool, with the least number of off-target sites, were compared and inspected using the BLAT tool of the UCSC genome browser to ensure minimal overlap between gRNAs and optimal placement near DNase hypersensitive regions(*46*). A total of 6 gRNAS were selected for validation *in vitro*, as well as a gRNA that does not target the human genome (non-target control/NTC). Oligos for ZNF865 gRNAs were synthesized by the University of Utah DNA/Peptide Synthesis core and ThermoFisher Scientific.

Downregulation gRNA design was performed as described above, using Genome Target Scan 2 (GT-Scan2) and ChopChop(*44, 45*). Briefly, a panel of 5 gRNAs were designed within the 5'-UTR and the promoter region up to 1000 bp upstream of the ZNF865 TSS. Oligos for ZNF865 gRNAs were synthesized by the University of Utah DNA/Peptide Synthesis core and ThermoFisher Scientific.

Cloning

gRNAs, and a non-target that does not target the human genome, were synthesized, annealed, phosphorylated, and ligated into individual U6-gRNA-UbC-DsRed-P2A-Bsr (upregulation gRNA) lentiviral upregulation expression vectors (Addgene, #83919) or KRAB CRISPRi downregulation expression vector pLV-hUbC-dCas9-KRAB-T2A-GFP (Addgene, #71237). Successful gRNA insertion was verified through Sanger sequencing(*47-49*).

Table 1: sgRNA primers for targeting the CRISPR system to ZNF865 and a nontarget control for upregulation and downregulation.

gRNAs	**Protospacer Sequence**
VPR-ZNF865 Guide 1	CCGCACAAGGATGGATGAGT
VPR-ZNF865 Guide 2	GACGCCCAGAGCGTGTCGCG
VPR-ZNF865 Guide 3	GAGGCGGGCATTCAAAGCGC
VPR-ZNF865 Guide 4	TCGCCCACCGGAATCGGCCC
VPR-ZNF865 Guide 5	ATCCTCCACGCCGGCGCCTC
VPR-ZNF865 Guide 6	ACTTCCGCTTCCGGGCGGGC
KRAB-ZNF865 Guide 1	ATGGGGGCGCACGACTGCTA
KRAB-ZNF865 Guide 2	GACGCCCAGAGCGTGTCGCG
KRAB-ZNF865 Guide 3	TCGCCCACCGGAATCGGCCC
KRAB-ZNF865 Guide 4	CCATGCGGAATAGAAGCCCT
KRAB-ZNF865 Guide 5	GATTATAGCGATTATATGAG
Non-target	TTTTTAATACAAGGTAATCT

Harvesting of primary hNPCs and culture

Human healthy and degenerative nucleus pulposus tissues were obtained from surgical tissue waste from trauma patients with no history of back pain, and patients undergoing surgical treatment for back pain respectively. Briefly, NP tissue was rinsed twice with washing medium (DMEM-HG, 165 μg/mL gentamicin sulfate, 100μg/mL kanamycin sulfate, 1.25μg/mL amphotericin), minced, and enzymatically digested in washing medium with 0.3% (w/v) collagenase type II (Worthington Biochemical), 0.2% pronase (Sigma), and 5% FBS (ThermoFisher Scientific) for 2-3 hours at 37°C with 5% CO_2 under gentle agitation (*48*).

Isolated cells were passed through a 70μm cell strainer and washed twice. Cells were counted and plated at a density of 10,000 cells/cm^2 in NP cell culture medium (DMEM-HG with 10% FBS, 50μg/mL gentamicin, 25mM HEPES) supplemented with fresh 2ng/mL fibroblast growth factor-2 (FGF-2) (Peprotech). Cells were cultured in this medium at 37°C and 5% CO_2 in a humidified atmosphere and subcultured to 90% confluency, as previously described(*48*).

Lentivirus production

The gRNA plasmid DNA was used to produce lentivirus, as previously described(*47-49*). The amplified gRNA plasmid DNA was co-transfected into HEK 293T cells with psPAX2 (Addgene, plasmid #12260) and pMD2.G (Addgene, plasmid #12259) lentiviral packaging plasmids to create a lentivirus, as previously described[45]. Briefly, HEK 293T cells were seeded at a density of 62,500 cells/cm^2. The following day, lentiviral plasmids were added to the cells with Lipofectamine 2000 (ThermoFisher Scientific), following the manufacturer's protocol. After 24 hours, the cell supernatant was discarded and replaced with fresh medium. Cell supernatant containing the lentiviral vectors was collected at 48 and 72 hours, concentrated to 100X, and stored at -80°C until use(*49*).

dCas9-VPR upregulation transduction

HEK 293/ASC: HEK 293 cells and ASCs were plated at a density of 20,000 cells/cm^2 and 5,000 cells/cm^2, respectively, allowed to attach overnight, and transduced with EF-1α-dCas9-VPR-PuroR (dCas9-VPR) (Addgene, #99373) lentivirus, (1:20 dilution) in growth medium containing 4μg/mL polybrene, the following day. Both cell types were subjected to antibiotic selection (1μg/mL) over the course of 3 days to select for dCas9-VPR expressing cells. *hNPCs:* hNPCs (p1-p2) were plated at a density of 20,000 cells/cm^2, allowed to attach overnight, and transduced with EF-1a-dCas9-VPR-eGFP (Addgene, #241307) lentivirus, (1:2 dilution) in growth medium containing 4μg/mL polybrene, the following day. 72-hours following transduction hNPCs were subjected to fluorescence activated cells sorting (FACS) to select for GFP+ expressing cells.

After dCas9-VPR transduction, dCas9-VPR expressing HEK 293 cells, hNPCs, and ASCs were transduced with gRNA targeting lentiviral vectors. *HEK293-VPR:* HEK 293-VPR cells were plated at a density of 20,000 cells/cm^2 and transduced with gRNA vector (1:250 dilution) targeting ZNF865 (Addgene, #241309) or non-target the following day in complete media. *hNPC-VPR*: hNPCs were plated at a density of 5,000 cells/cm^2 in a 24-well plate and transduced with gRNA vector (1:160 dilution) targeting ZNF865 (Addgene, #241309) or non-target in complete media the following day. *ASC-VPR*: hNPCs were plated at a density of 5,000 cells/cm^2 in a 24-well plate and transduced with gRNA vectors (1:160 dilution) targeting ZNF865 (Addgene, #241309), or non-target in complete media the following day. Transduced HEK 293, ASCs and hNPCs were examined for fluorescence after 72 hours and showed near 100% transduction efficiency.

dCas9-KRAB downregulation transduction

For ZNF865 downregulation, naïve HEK-293, naïve ASCs, and naïve hNPCs were plated at a density of 20,000 cells/cm^2, 5,000 cells/cm^2, or 10,000 cells/cm^2 respectively, in 24-well plates and allowed to attach overnight. The following day, 100X sgRNA targeting ZNF865 (Addgene, #241308) or non-target virus was diluted 1:16 in complete growth medium supplemented with 4μg/mL polybrene and used to transduce cells. Cells were examined for fluorescence after 72-hours and showed near 100% transduction efficiency.

qRT-PCR

Successfully transduced cells were analyzed for changes in ZNF865 gene expression by qRT-PCR (n=4). 72-hours post-transduction, RNA was isolated and harvested using the Quick-RNA Micro Kit (Zymo Research, R1051), complementary DNA (cDNA) was synthesized from the purified RNA with high-capacity cDNA reverse transcription kit with RNAse inhibitor (Applied Biosystems). cDNA was then used for qRT-PCR with TaqMan gene expression assays (ThermoFisher) for ZNF865 (Hs05052648_s1). Beta-2-microglobulin (B2M, Hs00187842_m1) was used as an internal standard and changes in ZNF865 expression was normalized to B2M expression(*50*). Fold-change in mRNA expression relative to the non-target or ZNF865 edited cells was calculated using the ΔΔCT method.

RNA-sequencing

RNA-sequencing (RNAseq) was utilized to evaluate differential gene expression due to ZNF865 upregulation. HEK 293 cells, ASCs, and primary human NP cell samples (**Table** S4) were analyzed for global changes in gene expression after modification with ZNF865 or NTC CRISPRa vectors. Briefly, Total RNA was isolated from samples using a Quick-RNA Kit (Zymo Research,

Irvine, CA). Isolated Total RNA (100-1000ng) was prepared using an Illumina TruSeq Stranded mRNA Library Prep Kit with PolyA Selection and samples were submitted to the High-Throughput Genomics Shared Resource Core at the Huntsman Cancer Institute for sequencing on a NovaSeq 6000, utilizing a NovaSeq Reagent Kit v1.5_150x150bp sequencing with 33 million reads per sample.

Using previously described methods, data were normalized and compared to non-target control cells(*47, 48*). Sequencing reads were aligned to the hg38 build of the human genome using HISAT2 (*51*)and SAMtools (*52*) was used to convert SAM files to BAM files. Genes were defined by the University of California Santa Cruz (UCSC) Known Genes, and reads mapping to known genes were assigned using featureCounts from the SubRead package(*53, 54*). Reads were normalized and differential analysis was performed using EdgeR (*55*) (**Figure 1E-1G**) or the DESeq2 package in R (**Figure 6A**)(*53, 56*). We used an adjusted p-value threshold of <0.05 to identify genes that were significantly up- or down-regulated when comparing patient samples in Figure 6. Enriched GO biological and molecular processes were determined from lists of significantly differentially expressed genes using Enrichr (*31, 57*).

Single cell RNA-sequencing

Single cell RNA sequencing (scRNA-seq) previously performed in *Jacobsen et al.* was mined for the relationship of ZFP865, the identified orthologue of human ZNF865(*33*), with aging in mice. In this study, mice were used at three ages: 4 months (skeletal maturity), 12 months (equivalent to human age with peak back pain disability), and 24 months (equivalent to human age with peak back pain prevalence)(*43*). Cells were isolated from 6 whole naïve coccygeal IVDs per mouse, from 6 mice per age group and pooled. Samples were processed by the Genomics Core

Facility at the Icahn School of Medicine at Mount Sinai. Samples were processed using the 10X Genomics Chromium 3' Kit and sequenced using an Illumina S1 NovaSeq chip. Cell Ranger software mapped reads to mouse mm10-2020-A reference genome. Data was processed via Seurat including quality control filtering, normalization, and unsupervised clustering. Cell clusters were visualized with uniform manifold approximation and projection (UMAP). Differential gene expression analysis identified gene markers for individual clusters and canonical markers facilitated annotation of clusters. Data was subset to NP and Notochordal clusters for analysis of ZFP865 expression. ZFP865 expression level was determined at the cellular level for each age, percentage of cells positively expressing ZFP865 at each age was also determined.

Cell proliferation quantification

Following successful transduction, HEK 293, ASCs, hNPCs, cells transduced with either the CRISPRa upregulation system or CRISPRi downregulation system (n=4) were evaluated for cell proliferation over the course of 3-10 days. Individual cells were counted using ImageJ or a hemacytometer(*58*). Briefly, fluorescing cell counts were obtained by uploading images into a stack and thresholding the images to ensure only individual cells are shown within the image. After thresholding, cell counts were obtained by analyzing particles, generating a mask, and then counting the masks generated while excluding cells on the edges of the image. In instances where cell density was too great for thresholding and visually isolating individual cells, cells were manually counted in ImageJ using the cell counter plugin(*58*).

Immunofluorescence ($P16^{INK4A}$, $p21^{CIP1}$ and ZNF865)

Primary hNPCs were plated into cell culture chamber slides at a concentration of 10,000 cells/cm^2 and then transduced with the ZNF865 or NTC downregulation expression cassettes. Cells were then cultured for 10 or 24 days after which the cells were fixed with 10% formalin. Following fixation cells were permeabilized with 0.2% Triton X in PBS for 5 min. Cells were then washed three times with PBS and treated with blocking solution (5% goat serum [MP Biomedicals] in PBS for 1 hour at room temperature). Following treatment with blocking solution, the blocking solution was removed, and the cells were treated with primary antibody; p16^{INK4A} (p16) antibody (1:100 in 1% BSA in PBS; Proteintech), p21^{CIP1} (p21) antibody (1:100 in 1% BSA in PBS; Proteintech) or ZNF865 (1:100 in 1% BSA in PBS; Atlas Antibodies), normal rabbit IgG (Invitrogen) or BSA only negative controls and incubated at room temperature for 2 hours. Following incubation cells were washed three times with PBS, treated with goat anti-rabbit Coralite 594 (1:100 Proteintech) in 1% BSA in PBS, and incubated for 1 hour at room temperature. Subsequently, cells were rinsed three times with PBS, treated with DAPI solution (3ng/mL) for 10 minutes, and mounted with Vectamount Mounting Medium prior to fluorescence imaging (Olympus IX73).

Alkaline comet assay

The alkaline comet assay was used to assess DNA damage in primary human NP cells. NP cells were trypsinized and resuspended in cold PBS at 1 x 10^6 cells per mL. 5 x 10^4 NP cells were mixed in a 3:7 volume ratio with 1% Low Melting Point Agarose (BP1360, Fisher Scientific). The mixture was then applied to a Superfrost Plus slide (12-550-15, Fisher Scientific) precoated with 1% normal melting point agarose (20-102, Apex). The slides were then transferred to the lysis solution (2.5 M NaCl, 100 mM disodium EDTA, 10 mM Tris Base, 1% Triton X, pH 10) and allowed to lyse overnight at 4˚C in the dark. Immediately following lysis, the slides were washed

1x with dH_2O and immersed in an electrophoresis tank containing alkaline electrophoresis solution (300 mM NaOH, 1 mM disodium EDTA, pH >13) for 30 min followed by electrophoresis at 1 V/cm for 20 min at 300 mA. Slides were then washed for 10 minutes in PBS and an additional 10 minutes in dH_2O at 4˚C and allowed to dry at RT overnight. Dried slides were then stained with 1ug/mL DAPI (62248, Thermo Fisher Scientific). At least 100 randomly selected stained nuclei per slide were imaged under an Olympus IX73 microscope. Comets were analyzed in ImageJ using the OpenComet plugin(*59*).

SA-β-Galactosidase staining

Primary hNPCs were plated in a 24-well plate at a concentration of 10,000 cells/cm^2 and allowed to attach overnight. The following day attached cells were transduced with the ZNF865 (Guide 2 and Guide 3) or NTC downregulation expression cassettes. Cells were cultured for 10 or 24 days, at which point they were fixed and stained for SA-β-galactosidase using a Senescent Cell Histochemical Staining Kit (Sigma-Aldrich, CS0030-1KT). Cellular senescence was quantified by counting SA-β-galactosidase stained and unstained cells using ImageJ.

Custom Luminex assay

Following upregulation of ZNF865 in primary dhNPCs a custom Luminex panel (Procartaplex 11 analyte multiplexed assay, Thermo Fisher) was run for IL1-β, IL-6, IL-8(CXCL8), TNF-α, MCP-1(CCL2), MMP-1,MMP-12, MMP-3, MMP-8, NGF-β, VEGF-a. 10-14 days following transduction of dhNPCs with ZNF865-VPR or NT, degenerative and healthy samples were passaged and plated in T-25 flasks at the appropriate cell density and 3 mL of media added per flask. 3 days following, supernatant was collected and spun at 1400 rpm for 10 minutes

to remove particulates, then aliquoted for storage at -80˚C until use. Images were taken at the same time point as collection for normalization based on cell number. The Procartaplex plate was then run according to the manufacturer's instructions using 50 µl of supernatant per sample per well and run on a Luminex Magpix. Each sample was run in duplicate. After running the plate, values were then averaged across each duplicate and divided by the cell density to account for differences in cell numbers. Values below the detection range were given concentrations of ½ the detection limit of each analyte. ZNF865-VPR dhNPC values were then normalized to the non-target across individual patients before averaging across all patients to get a normalized concentration for each analyte. A composite SASP score weighting each analyte equally was then calculated by normalizing each analyte to the highest concentration measured across all samples, then taking the sum across all analytes to get a composite score for each sample.

Pellet Culture of dhNPCs

To evaluate extracellular matric ECM deposition in the ZNF865 edited cells, 3D pellet cultures were performed. ZNF865-VPR dhNPCs and non-target dhNPCs were passaged and resuspended at 1.25 million cells/mL in serum free growth medium. Serum free media consisted of DMEM-HG with pyruvate (Thermo), 0.1 µm dexamethasone, 1% antibiotic/antimycotic, 0.17mM ascorbic acid 2-phosphate, 0.35mM proline and 1% ITS+. Due to low cell numbers, three non-target dhNPC samples were pooled to form a single non-target dhNPC group. 200 µL aliquots of cell suspension was pipetted into individual wells of 96-well v-bottom plate and spun at 270G for 10 min at 4˚C. Cells were allowed to contract for 48 hrs to form pellets. Pellets were then gently lifted from the bottom of the plate. Media was changed every 3 days for 21 days and supernatant collected during every media change.

Pellet biochemical analysis

The total amount of collagen content within papain digested pellets and supernatant was analyzed using a modified hydroxyproline assay as previously described (*28, 49*). The total amount of DNA and GAG content within papain digested pellets and supernatant was analyzed using a previously described Hoescht dye assay and dimethylmethylene blue (DMMB) assay, respectively (*28, 49, 60, 61*). A composite anabolic score weighting the contributions of collagen and GAG equally by normalizing to the highest concentration measured across all samples, then taking the sum of each normalized collagen and GAG score to get a complete anabolic score. These were then normalized to the average non-target dhNPC value.

ATAC-sequencing

Primary patient samples (**Table S5**) were prepared in technical duplicate, where 50,000 cells per replicate were taken from cryogenically frozen vials and centrifuged at 500 x g for 5 minutes at 4°C. The supernatant was aspirated, and the resulting cell pellet was washed with 250 µL of ice-cold 1X PBS, pH 7.4 (Thermo Scientific; 10010072). The cells were then centrifuged at 500 x g for 5 minutes at 4°C, the supernatant was aspirated, and the resulting cell pellet was resuspended in 50 µL of lysis buffer containing the following: 10 mM Tris-HCl, pH 7.4 (Sigma-Aldrich; T2194), 3 mM $MgCl_2$ (Sigma-Aldrich; M1028), 10 mM NaCl (Sigma-Aldrich; 71386), 0.1% NP-40 (Millipore Sigma; 492016), 0.1% Tween-20 (Bio-Rad; 1610781), and 0.01% digitonin (Invitrogen; BN20061). Samples were then lysed via incubation on ice for 15 minutes and centrifuged at 500 x g for 5 minutes at 4°C. Following lysis, 1 mL of wash buffer (10 mM Tris-HCl, pH 7.4, 3 mM $MgCl_2$, 10 mM NaCl, and 0.1% Tween-20) was added to each sample,

which was then centrifuged at 500 x g for 5 minutes at 4°C. The supernatant was aspirated, and the resulting cell pellet was resuspended a second time in 1 mL of wash buffer. To pellet nuclei, cells were centrifuged at 500 x g for 10 minutes at 4°C. The supernatant was aspirated, and each resulting nuclei pellet was resuspended in transposition buffer containing the following: 10 mM Tris-HCl, pH 8.0, 5 mM $MgCl_2$, 10% Dimethylformamide (Fisher Bioreagents; BP1160), and 1 µL of TDE1 Tagment DNA enzyme per sample (Illumina; 20034197) diluted in PBS, pH 7.4.

For the transposition reaction, nuclei were incubated at 37°C for 30 minutes in an Eppendorf ThermoMixer C (EP5382000015) set to rotate at 1000 RPM. Following transposition, DNA was purified using the Zymo DNA Clean & Concentrator-5 kit (D4014) according to the manufacturer's instructions with a binding buffer to sample ratio of 5:1. The purified DNA was then amplified by PCR using a final concentration of 1X Phusion Master Mix (New England Biolabs; M0530), and 200 nM each of forward and reverse barcode primers. Amplified libraries were purified using a 1:1 volume ratio of AMPure XP beads (Beckman Coulter; A63882) and fragment size distribution and quality were assessed using a High-Sensitivity D1000 ScreenTape assay.

Libraries were sequenced on a NovaSeq X at a depth of ~50 million reads/sample and 100 bases from the 3' end of each read were trimmed using seqtk(*62*) with the following parameters: trimfq -e 100. Trimmed reads were then aligned to the hg38 build of the human genome using Bowtie(*63*) with the following parameters: --chunkmbs 512 -m 1 -t --best -q -S -l 32 -e 80 -n 2. SAM files were converted into BAM files and sorted using SAMtools(*52*). Peaks representing regions of accessible chromatin were called using MACS2(*64*) with an adjusted P-value cutoff of <0.05 and an mfold parameter between 15 and 100. FeatureCounts(*54*) was used to quantify reads that aligned to ATAC-seq peaks called across all samples. Reads were normalized and chromatin

regions displaying differential accessibility were identified using the DESeq2 package for R(*56*). To identify regions of chromatin with differential accessibility, we compared dhNPC samples to both hNPCs and ZNF865-VPR dhNPCs, and ZNF865-VPR dhNPCs to hNPCs.

Statistical Analysis

RNA-seq statistical analysis was performed and described in their respective sections (Enrichr, DESeq2, $\alpha=0.05$). Statistical analysis of qRT-PCR, Luminex, β-gal, p16, p21, Collagen, GAG, and Comets performed using JMP Pro or GraphPad Prism using a one-way ANOVA with Tukey's post hoc analysis. Statistical analysis for proliferation was performed using JMP Pro with a two-way ANOVA with Tukey's post hoc analysis. Expression level scRNA-seq data was determined to be non-normal, significant differences between ages were tested for using Kruskal-Wallis test with Dunn's comparisons and $p<0.05$ considered significant in GraphPad Prism. Simple linear regression and Pearsons's correlation were performed on percent positivity and age with $p<0.05$ considered significant.

List of Supplementary materials:

Table S1: KEGG Human Genome 2021 significant pathways (From RNAseq in *HEK293* cells) ZNF865-VPR versus NT.

Table S2: KEGG Human Genome 2021 significant pathways (From RNAseq in *ASC*s). ZNF865-VPR versus NT.

Table S3: KEGG Human Genome 2021 significant pathways (From RNAseq in dhNPCs) ZNF865 VPR dhNPCs vs Non Target dhNPCs

Table S4: RNAseq patient information

Table S5: ATACseq patient information

Supplementary Materials:

Table S1: KEGG Human Genome 2021 significant pathways (From RNAseq in *HEK293* cells) ZNF865-VPR versus NT.

Pathway	Adjusted p-value
Amyotrophic lateral sclerosis	5.55E-20
Pathways of neurodegeneration	4.13E-18
Alzheimer disease	6.48E-17
Parkinson disease	1.02E-16
Oxidative phosphorylation	1.74E-16
Huntington disease	5.45E-16
Prion disease	3.79E-13
Spliceosome	3.55E-10
Diabetic cardiomyopathy	2.26E-09
Thermogenesis	6.03E-09
Cell cycle	1.25E-08
Non-alcoholic fatty liver disease	3.53E-08
p53 signaling pathway	5.40E-07
Cellular senescence	2.92E-06
RNA transport	4.39E-05
Salmonella infection	3.28E-04
Endocytosis	4.48E-04
DNA replication	4.99E-04
Shigellosis	7.44E-04
Autophagy	7.44E-04
Ubiquitin mediated proteolysis	0.001155331
Hepatocellular carcinoma	0.001315274
Spinocerebellar ataxia	0.001682104
Bacterial invasion of epithelial cells	0.001799459
Epstein-Barr virus infection	0.005002029
Mismatch repair	0.005002029
mRNA surveillance pathway	0.005002029
mTOR signaling pathway	0.006346221
Protein processing in endoplasmic reticulum	0.006346221
Glioma	0.007226928
Chronic myeloid leukemia	0.008454682
Apoptosis	0.010405806
Basal cell carcinoma	0.01195743
RNA degradation	0.013234801
Pathogenic Escherichia coli infection	0.013655447
Viral carcinogenesis	0.013655447
Longevity regulating pathway	0.015421792
Proteoglycans in cancer	0.015421792
Colorectal cancer	0.015421792
Small cell lung cancer	0.016643811
Cardiac muscle contraction	0.017180833
Nucleotide excision repair	0.020627196
Regulation of actin cytoskeleton	0.026414694
Breast cancer	0.026414694
Propanoate metabolism	0.026414694
Various types of N-glycan biosynthesis	0.02721576
Notch signaling pathway	0.02721576
Pentose phosphate pathway	0.029210609
Hepatitis B	0.033894794
Human T-cell leukemia virus 1 infection	0.042175878
Lysine degradation	0.048599192
FoxO signaling pathway	0.048599192
Yersinia infection	0.048599192
Endometrial cancer	0.048599192
Gastric cancer	0.048599192

Table S2: KEGG Human Genome 2021 significant pathways (From RNAseq in *ASC*s). ZNF865-VPR versus NT.

Pathway	Adjusted P-value	Pathway	Adjusted P-value
Cell cycle	1.76E-11	Sphingolipid signaling pathway	0.002706
Focal adhesion	2.90E-10	Relaxin signaling pathway	0.002706
Pathways in cancer	2.24E-09	Phosphatidylinositol signaling system	0.002836
Lysosome	2.51E-09	Amoebiasis	0.002874
Protein processing in endoplasmic reticulum	3.85E-09	Progesterone-mediated oocyte maturation	0.00323
DNA replication	3.85E-09	AMPK signaling pathway	0.003313
Human papillomavirus infection	3.61E-08	Thyroid hormone signaling pathway	0.004204
Amyotrophic lateral sclerosis	1.38E-07	Gastric cancer	0.004234
Salmonella infection	1.38E-07	Oocyte meiosis	0.004543
AGE-RAGE signaling pathway in diabetic complications	3.28E-07	Growth hormone synthesis, secretion and action	0.004591
Cellular senescence	3.64E-07	Human immunodeficiency virus 1 infection	0.004659
Pathways of neurodegeneration	5.23E-07	Glioma	0.005101
Human T-cell leukemia virus 1 infection	6.40E-07	Ubiquitin mediated proteolysis	0.005211
Shigellosis	6.90E-07	ErbB signaling pathway	0.005401
Endocytosis	9.00E-07	Hypertrophic cardiomyopathy	0.005469
Adherens junction	9.55E-07	Gap junction	0.006164
Proteoglycans in cancer	1.19E-06	Choline metabolism in cancer	0.006237
Diabetic cardiomyopathy	1.28E-06	Renal cell carcinoma	0.007005
Regulation of actin cytoskeleton	1.45E-06	Vibrio cholerae infection	0.007005
TGF-beta signaling pathway	2.08E-06	Leukocyte transendothelial migration	0.007454
Small cell lung cancer	2.11E-06	Ferroptosis	0.007454
Bacterial invasion of epithelial cells	2.11E-06	Apelin signaling pathway	0.007454
Autophagy	2.13E-06	Hippo signaling pathway	0.007543
Alzheimer disease	5.64E-06	Ras signaling pathway	0.007984
Neurotrophin signaling pathway	5.64E-06	Chagas disease	0.008369
Parkinson disease	6.83E-06	Lysine degradation	0.009647
Axon guidance	1.01E-05	Lipid and atherosclerosis	0.010094
Hepatocellular carcinoma	1.12E-05	Breast cancer	0.011048
ECM-receptor interaction	1.66E-05	Phospholipase D signaling pathway	0.013267
MAPK signaling pathway	1.91E-05	Kaposi sarcoma-associated herpesvirus infection	0.013474
Fluid shear stress and atherosclerosis	1.91E-05	Epstein-Barr virus infection	0.015663
Pancreatic cancer	2.75E-05	Thermogenesis	0.016597
Insulin resistance	3.30E-05	Epithelial cell signaling in Helicobacter pylori infection	0.016932
PI3K-Akt signaling pathway	3.64E-05	Viral carcinogenesis	0.017764
Mitophagy	3.64E-05	Wnt signaling pathway	0.018582
Apoptosis	4.55E-05	Parathyroid hormone synthesis, secretion and action	0.019003
FoxO signaling pathway	5.99E-05	Melanogenesis	0.019402
Huntington disease	6.82E-05	Dilated cardiomyopathy	0.019753
Human cytomegalovirus infection	1.34E-04	Vasopressin-regulated water reabsorption	0.020232
Base excision repair	1.53E-04	Citrate cycle (TCA cycle)	0.020232
mTOR signaling pathway	1.72E-04	C-type lectin receptor signaling pathway	0.020463
Fanconi anemia pathway	1.76E-04	Alanine, aspartate and glutamate metabolism	0.020463
Hepatitis B	1.96E-04	Toxoplasmosis	0.021236
Longevity regulating pathway	2.09E-04	RNA degradation	0.022609
Rap1 signaling pathway	2.18E-04	Other types of O-glycan biosynthesis	0.023746
Spinocerebellar ataxia	2.18E-04	Non-alcoholic fatty liver disease	0.024677
Inositol phosphate metabolism	2.90E-04	Arrhythmogenic right ventricular cardiomyopathy	0.025104
Prion disease	2.90E-04	SNARE interactions in vesicular transport	0.025333
Estrogen signaling pathway	3.01E-04	Tight junction	0.026773
Pathogenic Escherichia coli infection	3.26E-04	Cysteine and methionine metabolism	0.027314
Homologous recombination	4.35E-04	Inflammatory mediator regulation of TRP channels	0.027314
RNA transport	4.52E-04	Regulation of lipolysis in adipocytes	0.027371
Mismatch repair	4.52E-04	Central carbon metabolism in cancer	0.027371
TNF signaling pathway	4.52E-04	RNA polymerase	0.027371
Aldosterone synthesis and secretion	4.97E-04	GnRH signaling pathway	0.027371
Cushing syndrome	6.32E-04	cGMP-PKG signaling pathway	0.028104
p53 signaling pathway	6.32E-04	Endometrial cancer	0.030745
Prostate cancer	7.52E-04	Measles	0.03469
Purine metabolism	8.47E-04	Pyrimidine metabolism	0.03469
Nucleotide excision repair	9.53E-04	Other glycan degradation	0.034719
Colorectal cancer	9.56E-04	Ribosome biogenesis in eukaryotes	0.038753
Phagosome	9.56E-04	VEGF signaling pathway	0.038753
HIF-1 signaling pathway	0.001439	Platelet activation	0.039293
Fc gamma R-mediated phagocytosis	0.001482	Signaling pathways regulating pluripotency of stem cells	0.041146
Yersinia infection	0.001703	mRNA surveillance pathway	0.041518
Chronic myeloid leukemia	0.001703	Glutathione metabolism	0.043062
Glycosaminoglycan biosynthesis	0.001781	Oxidative phosphorylation	0.045129

Table S3: KEGG Human Genome 2021 significant pathways (From RNAseq in dhNPCs) ZNF865 VPR dhNPCs vs Non Target dhNPCs

Pathway	Adjusted p-value
Cell cycle	1.65E-10
DNA replication	1.68E-10
Pathways in cancer	4.12E-10
Protein digestion and absorption	1.53E-07
ECM-receptor interaction	1.04E-06
Focal adhesion	1.38E-06
PI3K-Akt signaling pathway	1.97E-05
Axon guidance	3.35E-05
Basal cell carcinoma	3.35E-05
Human papillomavirus infection	3.50E-05
Breast cancer	8.66E-05
AGE-RAGE signaling pathway in diabetic complications	9.73E-05
TGF-beta signaling pathway	1.00E-04
Hippo signaling pathway	2.31E-04
Gastric cancer	2.40E-04
Wnt signaling pathway	2.98E-04
Hepatocellular carcinoma	3.61E-04
Complement and coagulation cascades	5.53E-04
Fanconi anemia pathway	6.26E-04
p53 signaling pathway	6.26E-04
Colorectal cancer	0.001832
Bladder cancer	0.001864
Proteoglycans in cancer	0.002686
Prostate cancer	0.00292
Relaxin signaling pathway	0.003678
Cushing syndrome	0.004663
Cellular senescence	0.004987
Mismatch repair	0.005329
Homologous recombination	0.006129
Human T-cell leukemia virus 1 infection	0.007131
Small cell lung cancer	0.008761
Calcium signaling pathway	0.009037
Gap junction	0.013074
Acute myeloid leukemia	0.014962
Glycine, serine and threonine metabolism	0.016079
Progesterone-mediated oocyte maturation	0.019913
Arrhythmogenic right ventricular cardiomyopathy	0.019913
Melanogenesis	0.021449
Signaling pathways regulating pluripotency of stem cells	0.02368
MAPK signaling pathway	0.02454
Malaria	0.02454
Melanoma	0.02454
Ras signaling pathway	0.025465
Oocyte meiosis	0.026862
Fluid shear stress and atherosclerosis	0.03041
Amoebiasis	0.046035

Table S4: RNAseq patient information

Library number	Genotype	Sample name	Biological replicate	Technical replicate	Sex	Age	Sample designation
1	dhNPC	dhNPC 33 Y M	-	1	male	33	25852X3
2	dhNPC	dhNPC 33 Y M	-	2	male	33	25852X4
3	hNPC	hNPC 69 Y F	1	-	female	69	23965X3
4	hNPC	hNPC 32 Y F	2	-	female	32	23965X4
5	ZNF865-VPR dhNPC	ZNF865 VPR dhNPC 32 Y M	-	1	male	32	23965X5
6	ZNF865-VPR dhNPC	ZNF865 VPR dhNPC 32 Y M	-	2	male	32	23965X6

Table S5: ATACseq patient information

library number	genotype	sample name	technical replicate	sex	age	sample designation
1	hNPCs	atac_hnpc_r1	1	female	69	23835X1
2	dhNPCs	atac_dhnpc_r1	1	male	60	23835X2
3	ZNF865-dhNPCs	atac_znf865_dhnpc_r1	1	male	32	23835X3
4	hNPCs	atac_hnpc_r2	2	female	69	23835X4
5	dhNPCs	atac_dhnpc_r2	2	male	60	23835X5
6	ZNF865-dhNPCs	atac_znf865_dhnpc_r2	2	male	32	23835X6

References

1. W. Huang, L. J. Hickson, A. Eirin, J. L. Kirkland, L. O. Lerman, Cellular senescence: the good, the bad and the unknown. *Nature Reviews Nephrology* **18**, 611-627 (2022).
2. S. Özcan, N. Alessio, M. B. Acar, E. Mert, F. Omerli, G. Peluso, U. Galderisi, Unbiased analysis of senescence associated secretory phenotype (SASP) to identify common components following different genotoxic stresses. *Aging (Albany NY)* **8**, 1316-1329 (2016).
3. J. P. Coppé, P. Y. Desprez, A. Krtolica, J. Campisi, The senescence-associated secretory phenotype: the dark side of tumor suppression. *Annu Rev Pathol* **5**, 99-118 (2010).
4. V. Lau, L. Ramer, M.-È. Tremblay, An aging, pathology burden, and glial senescence build-up hypothesis for late onset Alzheimer's disease. *Nature Communications* **14**, 1670 (2023).
5. Y. Ma, M. L. Erb, D. J. Moore, Aging, cellular senescence and Parkinson's disease. *Journal of Parkinson's Disease* **15**, 239-254 (2025).
6. M. J. Schafer, T. A. White, K. Iijima, A. J. Haak, G. Ligresti, E. J. Atkinson, A. L. Oberg, J. Birch, H. Salmonowicz, Y. Zhu, D. L. Mazula, R. W. Brooks, H. Fuhrmann-Stroissnigg, T. Pirtskhalava, Y. S. Prakash, T. Tchkonia, P. D. Robbins, M. C. Aubry, J. F. Passos, J. L. Kirkland, D. J. Tschumperlin, H. Kita, N. K. LeBrasseur, Cellular senescence mediates fibrotic pulmonary disease. *Nature Communications* **8**, 14532 (2017).
7. R. Okuda, K. Aoshiba, H. Matsushima, T. Ogura, K. Okudela, K. Ohashi, Cellular senescence and senescence-associated secretory phenotype: comparison of idiopathic pulmonary fibrosis, connective tissue disease-associated interstitial lung disease, and chronic obstructive pulmonary disease. *J Thorac Dis* **11**, 857-864 (2019).
8. N. Surmachevska, J. Rubio, Senescence in Osteoarthritis: Overview of Mechanisms and Therapeutics. *Eur J Rheumatol* **11**, S3-6 (2023).
9. F. Wang, F. Cai, R. Shi, X. H. Wang, X. T. Wu, Aging and age related stresses: a senescence mechanism of intervertebral disc degeneration. *Osteoarthritis and Cartilage* **24**, 398-408 (2016).
10. M. E. Copp, S. Chubinskaya, D. N. Bracey, J. Shine, G. Sessions, R. F. Loeser, B. O. Diekman, Comet assay for quantification of the increased DNA damage burden in primary human chondrocytes with aging and osteoarthritis. *Aging Cell* **21**, e13698 (2022).
11. T. Vos, Global, regional, and national incidence, prevalence, and years lived with disability for 301 acute and chronic diseases and injuries in 188 countries, 1990-2013: a systematic analysis for the Global Burden of Disease Study 2013. *Lancet* **386**, 743-800 (2015).
12. D. I. Rubin, Epidemiology and risk factors for spine pain. *Neurol Clin* **25**, 353-371 (2007).
13. S. Baliga, K. Treon, N. J. Craig, Low Back Pain: Current Surgical Approaches. *Asian Spine J* **9**, 645-657 (2015).
14. K. M. Cheung, J. Karppinen, D. Chan, D. W. Ho, Y. Q. Song, P. Sham, K. S. Cheah, J. C. Leong, K. D. Luk, Prevalence and pattern of lumbar magnetic resonance imaging

changes in a population study of one thousand forty-three individuals. *Spine (Phila Pa 1976)* **34**, 934-940 (2009).
15. G. Livshits, M. Popham, I. Malkin, P. N. Sambrook, A. J. Macgregor, T. Spector, F. M. Williams, Lumbar disc degeneration and genetic factors are the main risk factors for low back pain in women: the UK Twin Spine Study. *Ann Rheum Dis* **70**, 1740-1745 (2011).
16. M. Szpalski, R. Gunzburg, Lumbar spinal stenosis in the elderly: an overview. *European Spine Journal* **12**, S170-S175 (2003).
17. J. R. Meakin, J. S. Gregory, R. M. Aspden, F. W. Smith, F. J. Gilbert, The intrinsic shape of the human lumbar spine in the supine, standing and sitting postures: characterization using an active shape model. *J Anat* **215**, 206-211 (2009).
18. N. Kos, L. Gradisnik, T. Velnar, A Brief Review of the Degenerative Intervertebral Disc Disease. *Med Arch* **73**, 421-424 (2019).
19. H. E. Gruber, J. A. Ingram, H. J. Norton, E. N. J. Hanley, Senescence in Cells of the Aging and Degenerating Intervertebral Disc: Immunolocalization of Senescence-Associated β-Galactosidase in Human and Sand Rat Discs. *Spine* **32**, 321-327 (2007).
20. S. Roberts, E. H. Evans, D. Kletsas, D. C. Jaffray, S. M. Eisenstein, Senescence in human intervertebral discs. *Eur Spine J* **15 Suppl 3**, S312-316 (2006).
21. B. R. Whatley, X. Wen, Intervertebral disc (IVD): Structure, degeneration, repair and regeneration. *Materials Science and Engineering: C* **32**, 61-77 (2012).
22. Z. I. Johnson, Z. R. Schoepflin, H. Choi, I. M. Shapiro, M. V. Risbud, Disc in flames: Roles of TNF-α and IL-1β in intervertebral disc degeneration. *Eur Cell Mater* **30**, 104-116; discussion 116-107 (2015).
23. G.-Z. Zhang, M.-Q. Liu, H.-W. Chen, Z.-L. Wu, Y.-C. Gao, Z.-J. Ma, X.-G. He, X.-W. Kang, NF-κB signalling pathways in nucleus pulposus cell function and intervertebral disc degeneration. *Cell Proliferation* **54**, e13057 (2021).
24. H. Cherif, D. G. Bisson, P. Jarzem, M. Weber, J. A. Ouellet, L. Haglund, Curcumin and o-Vanillin Exhibit Evidence of Senolytic Activity in Human IVD Cells In Vitro. *J Clin Med* **8**, (2019).
25. H. Cherif, D. G. Bisson, M. Mannarino, O. Rabau, J. A. Ouellet, L. Haglund, Senotherapeutic drugs for human intervertebral disc degeneration and low back pain. *Elife* **9**, (2020).
26. M. Mannarino, H. Cherif, S. Ghazizadeh, O. W. Martinez, K. Sheng, E. Cousineau, S. Lee, M. Millecamps, C. Gao, A. Gilbert, C. Peirs, R. S. Naeini, J. A. Ouellet, L. S. Stone, L. Haglund, Senolytic treatment for low back pain. *Science Advances* **11**, eadr1719 (2025).
27. E. J. Novais, V. A. Tran, S. N. Johnston, K. R. Darris, A. J. Roupas, G. A. Sessions, I. M. Shapiro, B. O. Diekman, M. V. Risbud, Long-term treatment with senolytic drugs Dasatinib and Quercetin ameliorates age-dependent intervertebral disc degeneration in mice. *Nat Commun* **12**, 5213 (2021).
28. H. Levis, C. Lewis, M. Fainor, A. Lawal, E. Stockham, J. Weston, N. Farhang, S. E. Gullbrand, R. D. Bowles, Targeted CRISPR regulation of ZNF865 enhances stem cell

cartilage deposition, tissue maturation rates, and mechanical properties in engineered intervertebral discs. *Acta Biomater* **191**, 276-291 (2025).
29. S. Frietze, P. J. Farnham, Transcription factor effector domains. *Subcell Biochem* **52**, 261-277 (2011).
30. in *Undiagnosed Disease Network* (Undiagnosed Disease Network Undiagnosed Disease Network 2021), vol. 2025.
31. M. V. Kuleshov, M. R. Jones, A. D. Rouillard, N. F. Fernandez, Q. Duan, Z. Wang, S. Koplev, S. L. Jenkins, K. M. Jagodnik, A. Lachmann, M. G. McDermott, C. D. Monteiro, G. W. Gundersen, A. Ma'ayan, Enrichr: a comprehensive gene set enrichment analysis web server 2016 update. *Nucleic Acids Res* **44**, W90-97 (2016).
32. M. Kanehisa, S. Goto, KEGG: kyoto encyclopedia of genes and genomes. *Nucleic Acids Res* **28**, 27-30 (2000).
33. J. R. Smith, G. T. Hayman, S. J. Wang, S. J. F. Laulederkind, M. J. Hoffman, M. L. Kaldunski, M. Tutaj, J. Thota, H. S. Nalabolu, S. L. R. Ellanki, M. A. Tutaj, J. L. De Pons, A. E. Kwitek, M. R. Dwinell, M. E. Shimoyama, The Year of the Rat: The Rat Genome Database at 20: a multi-species knowledgebase and analysis platform. *Nucleic Acids Res* **48**, D731-d742 (2020).
34. A. Chavez, J. Scheiman, S. Vora, B. W. Pruitt, M. Tuttle, P. R. I. E, S. Lin, S. Kiani, C. D. Guzman, D. J. Wiegand, D. Ter-Ovanesyan, J. L. Braff, N. Davidsohn, B. E. Housden, N. Perrimon, R. Weiss, J. Aach, J. J. Collins, G. M. Church, Highly efficient Cas9-mediated transcriptional programming. *Nat Methods* **12**, 326-328 (2015).
35. P. I. Thakore, A. M. D'Ippolito, L. Song, A. Safi, N. K. Shivakumar, A. M. Kabadi, T. E. Reddy, G. E. Crawford, C. A. Gersbach, Highly specific epigenome editing by CRISPR-Cas9 repressors for silencing of distal regulatory elements. *Nat Methods* **12**, 1143-1149 (2015).
36. R. Kandhaya-Pillai, F. Miro-Mur, J. Alijotas-Reig, T. Tchkonia, J. L. Kirkland, S. Schwartz, TNFα-senescence initiates a STAT-dependent positive feedback loop, leading to a sustained interferon signature, DNA damage, and cytokine secretion. *Aging (Albany NY)* **9**, 2411-2435 (2017).
37. Y. Tanigawa, E. S. Dyer, G. Bejerano, WhichTF is functionally important in your open chromatin data? *PLoS Comput Biol* **18**, e1010378 (2022).
38. H. M. Song, Z. W. Li, Q. Huang, C. G. Wu, M. H. Li, J. K. Shen, A diagnostic signatures for intervertebral disc degeneration using TNFAIP6 and COL6A2 based on single-cell RNA-seq and bulk RNA-seq analyses. *Ann Med* **57**, 2443568 (2025).
39. C. Tseng, B. Chen, Y. Han, K. Wang, Q. Song, H. Shen, Z. Chen, Advanced glycation end products promote intervertebral disc degeneration by transactivation of matrix metallopeptidase genes. *Osteoarthritis and Cartilage* **32**, 187-199 (2024).
40. M. Uhlén, L. Fagerberg, B. M. Hallström, C. Lindskog, P. Oksvold, A. Mardinoglu, Å. Sivertsson, C. Kampf, E. Sjöstedt, A. Asplund, I. Olsson, K. Edlund, E. Lundberg, S. Navani, C. A.-K. Szigyarto, J. Odeberg, D. Djureinovic, J. O. Takanen, S. Hober, T. Alm, P.-H. Edqvist, H. Berling, H. Tegel, J. Mulder, J. Rockberg, P. Nilsson, J. M. Schwenk, M. Hamsten, K. von Feilitzen, M. Forsberg, L. Persson, F. Johansson, M. Zwahlen, G. von Heijne, J. Nielsen, F. Pontén, Tissue-based map of the human proteome. *Science* **347**, 1260419 (2015).

41. K. Hong, Q. Yang, H. Yin, N. Wei, W. Wang, B. Yu, Comprehensive analysis of ZNF family genes in prognosis, immunity, and treatment of esophageal cancer. *BMC Cancer* **23**, 301 (2023).
42. C. Liu, Y. Wang, J. W. Li, X. Zhu, H. S. Jiang, H. Zhao, L. M. Zhang, MiR-184 Mediated the Expression of ZNF865 in Exosome to Promote Procession in the PD Model. *Mol Neurobiol*, (2023).
43. H. T. Jacobsen T, Cavendish E, Laudier D, Han W, Huang A, Iatridis J, paper presented at the Transactions of the Orthopedic Research Society, Long Beach, CA, 2024.
44. A. O'Brien, T. L. Bailey, GT-Scan: identifying unique genomic targets. *Bioinformatics* **30**, 2673-2675 (2014).
45. K. Labun, T. G. Montague, M. Krause, Y. N. Torres Cleuren, H. Tjeldnes, E. Valen, CHOPCHOP v3: expanding the CRISPR web toolbox beyond genome editing. *Nucleic Acids Res* **47**, W171-w174 (2019).
46. W. J. Kent, BLAT--the BLAST-like alignment tool. *Genome Res* **12**, 656-664 (2002).
47. N. Farhang, B. Davis, J. Weston, M. Ginley-Hidinger, J. Gertz, R. D. Bowles, Synergistic CRISPRa-Regulated Chondrogenic Extracellular Matrix Deposition Without Exogenous Growth Factors. *Tissue Engineering Part A* **26**, 1169-1179 (2020).
48. N. Farhang, M. Ginley-Hidinger, K. C. Berrett, J. Gertz, B. Lawrence, R. D. Bowles, Lentiviral CRISPR Epigenome Editing of Inflammatory Receptors as a Gene Therapy Strategy for Disc Degeneration. *Human Gene Therapy* **30**, 1161-1175 (2019).
49. N. Farhang, J. M. Brunger, J. D. Stover, P. I. Thakore, B. Lawrence, F. Guilak, C. A. Gersbach, L. A. Setton, R. D. Bowles, CRISPR-Based Epigenome Editing of Cytokine Receptors for the Promotion of Cell Survival and Tissue Deposition in Inflammatory Environments. *Tissue Engineering Part A* **23**, 738-749 (2017).
50. J. Vandesompele, K. De Preter, F. Pattyn, B. Poppe, N. Van Roy, A. De Paepe, F. Speleman, Accurate normalization of real-time quantitative RT-PCR data by geometric averaging of multiple internal control genes. *Genome Biology* **3**, research0034.0031 (2002).
51. D. Kim, J. M. Paggi, C. Park, C. Bennett, S. L. Salzberg, Graph-based genome alignment and genotyping with HISAT2 and HISAT-genotype. *Nature Biotechnology* **37**, 907-915 (2019).
52. H. Li, B. Handsaker, A. Wysoker, T. Fennell, J. Ruan, N. Homer, G. Marth, G. Abecasis, R. Durbin, The Sequence Alignment/Map format and SAMtools. *Bioinformatics* **25**, 2078-2079 (2009).
53. D. Kim, B. Langmead, S. L. Salzberg, HISAT: a fast spliced aligner with low memory requirements. *Nature Methods* **12**, 357-360 (2015).
54. Y. Liao, G. K. Smyth, W. Shi, featureCounts: an efficient general purpose program for assigning sequence reads to genomic features. *Bioinformatics* **30**, 923-930 (2014).
55. M. D. Robinson, D. J. McCarthy, G. K. Smyth, edgeR: a Bioconductor package for differential expression analysis of digital gene expression data. *Bioinformatics* **26**, 139-140 (2010).
56. M. I. Love, W. Huber, S. Anders, Moderated estimation of fold change and dispersion for RNA-seq data with DESeq2. *Genome Biol* **15**, 550 (2014).

57. E. Y. Chen, C. M. Tan, Y. Kou, Q. Duan, Z. Wang, G. V. Meirelles, N. R. Clark, A. Ma'ayan, Enrichr: interactive and collaborative HTML5 gene list enrichment analysis tool. *BMC Bioinformatics* **14**, 128 (2013).
58. C. A. Schneider, W. S. Rasband, K. W. Eliceiri, NIH Image to ImageJ: 25 years of image analysis. *Nature Methods* **9**, 671-675 (2012).
59. B. M. Gyori, G. Venkatachalam, P. S. Thiagarajan, D. Hsu, M.-V. Clement, OpenComet: An automated tool for comet assay image analysis. *Redox Biology* **2**, 457-465 (2014).
60. C. H. Zheng, M. E. Levenston, Fact versus artifact: avoiding erroneous estimates of sulfated glycosaminoglycan content using the dimethylmethylene blue colorimetric assay for tissue-engineered constructs. *Eur Cell Mater* **29**, 224-236; discussion 236 (2015).
61. Y. J. Kim, R. L. Sah, J. Y. Doong, A. J. Grodzinsky, Fluorometric assay of DNA in cartilage explants using Hoechst 33258. *Anal Biochem* **174**, 168-176 (1988).
62. H. Li. (Github).
63. B. Langmead, C. Trapnell, M. Pop, S. L. Salzberg, Ultrafast and memory-efficient alignment of short DNA sequences to the human genome. *Genome Biology* **10**, R25 (2009).
64. Y. Zhang, T. Liu, C. A. Meyer, J. Eeckhoute, D. S. Johnson, B. E. Bernstein, C. Nusbaum, R. M. Myers, M. Brown, W. Li, X. S. Liu, Model-based Analysis of ChIP-Seq (MACS). *Genome Biology* **9**, R137 (2008).

Acknowledgements

Research reported in this publication was supported by the National Institute of Health under award numbers R01 AR083990, R01 AR074998 and R01 AR080096. Sequencing was performed at the DNA Sequencing Core Facility, University of Utah. FACs was performed at the Flow Cytometry Core Facility, University of Utah. Research reported in this publication utilized the High-Throughput Genomics Shared Resource at the University of Utah and was supported by NIH/National Cancer Institute (NCI) award P30 CA042014. The content is solely the responsibility of the authors and does not necessarily represent the official views of the NIH.

Funding:

National Institute of Health grant R01 AR083990 (RDB)
National Institute of Health grant R01 AR074998 (RDB)
National Institute of Health grant R01 AR080096 (JCI)

Author Contributions

Conceptualization: CL, HL, JH, JTP, TDJ, SEG, BD, JG, RDB
Methodology: CL, HL, JH, JTP, BD, JG, RDB
Investigation: CL, HL, JH, JTP, TDJ
Visualization: CL, HL, JH, JTP, TDJ, RDB
Funding acquisition: RDB
Project administration: CL, RDB
Supervision: JCI, JG, RDB
Writing-original draft: CL, HL, JH, JTP, TDJ, RDB
Writing-review and editing: CL, HL, JH, JTP, TDJ, SEG, JCI, JG, BL, RDB

Competing interests:

Authors declare that they have no competing interests

Data and materials availability:

GEO accession # is pending due to government shutdown